ARTICLES
https://doi.org/10.1038/s41551-021-00768-z
nature biomedical engineering

Directly reprogrammed natural killer cells for cancer immunotherapy

Han-Seop Kim[1], Jae Yun Kim[1,2], Binna Seol[1], Cho Lok Song[1,2], Ji Eun Jeong[1] and Yee Sook Cho[1,2] ✉

Efficacious and accessible sources of natural killer (NK) cells would widen their use as immunotherapeutics, particularly for solid cancers. Here, we show that human somatic cells can be directly reprogrammed into NK cells with a CD56^{bright}CD16^{bright} phenotype using pluripotency transcription factors and an optimized reprogramming medium. The directly reprogrammed NK cells have strong innate–adaptive immunomodulatory activity and are highly potent against a wide range of cancer cells, including difficult-to-treat solid cancers and cancer stem cells. Both directly reprogrammed NK cells bearing a cancer-specific chimeric antigen receptor and reprogrammed NK cells in combination with antibodies competent for antibody-dependent cell-mediated cytotoxicity led to selective anticancer effects with augmented potency. The direct reprogramming of human somatic cells into NK cells is amenable to the production of autologous and allogeneic NK cells, and will facilitate the design and testing of cancer immunotherapies and combination therapies.

Immunotherapy using natural killer (NK) cells could overcome limitations of T cell anticancer immunotherapy and play an important role in cancer research and treatment[1]. In contrast with T cells, target cell recognition by NK cells is antigen nonspecific and is unrestricted by the major histocompatibility complex (MHC). Target cell recognition by NK cells is governed by a balance of multiple activating and inhibitory signals transduced by NK surface receptors (NKRs)[2,3]. Therefore, without previous priming or sensitization, NK cells can rapidly and effectively eradicate cancer cells lacking MHC class I expression, either directly through NK-mediated cytotoxicity or indirectly by releasing cytotoxic granules (containing granzymes and perforin, in particular) and immunoregulatory cytokines (such as interferon-γ (IFN-γ), tumour necrosis factor-α (TNF-α) and granulocyte–macrophage colony-stimulating factor) and chemokines (such as CCL3, CCL4 and RANTES)[2–4]. More importantly, NK cells can selectively kill quiescent or non-proliferating cancer stem cells (CSCs) associated with cancer resistance, reoccurrence and metastasis[5,6]. Therefore, these cells are considered a promising strategy for efficacious and lasting cancer treatment to prevent tumour metastasis and relapse.

The therapeutic potential of NK anticancer immunotherapy is dependent on multiple factors, including cell sources, the phenotypic repertoire of NKRs, the method of derivation and culture conditions. The main sources of NK cells include primary NK cells from peripheral blood (PB-NK cells), umbilical cord blood (UCB-NK cells) and bone marrow; differentiated NK cells from haematopoietic stem/progenitor cells (HSPCs) and pluripotent stem cells (PSCs); and immortalized clonal NK cell lines[1,3]. Phenotypically, NK cells are not homogeneous and generally can be classified into subpopulations on the basis of the relative expression of the markers CD56 (an adhesion molecule) and CD16 (FcγRIII; a type I transmembrane receptor for the Fc portion of immunoglobulin G (IgG))[4,7]. Functionally, CD56^{dim} NK cells are considered cytotoxic effectors, whereas CD56^{bright} NK cells are considered immunomodulatory effectors[8–10]. The two major subsets of blood-derived NK cells (that is, PB-NK cells and UCB-NK cells) are CD56^{dim}CD16^{bright} NK cells (~90%) and CD56^{bright}CD16$^{dim/-}$ NK cells (~10%)[8–10]. Notably, a subset of CD56^{bright}CD16^{bright} NK cells, which are mainly found in secondary lymphoid tissues[11], are a much rarer population than other CD56^{bright} cells[12,13] and remain substantially less studied. Studies have indicated ex vivo expansion of highly active CD56^{bright}CD16^{bright} NK cells and highlighted their therapeutic potential[14,15]. For wider and safer applications, the production of clinical-scale, homogeneous CD56^{bright}CD16^{bright} NK cells under feeder cell-free culture conditions has not been convincingly demonstrated to date.

The therapeutic effectiveness and safety of autologous and allogeneic NK cells has been reported in various haematological and solid cancers[3]; however, these treatments remain unsatisfactory, particularly in solid cancers. Recent studies elucidating NK alloreactivity increasingly support the use of allogeneic NK cells from healthy donors because of their favourable therapeutic outcomes and cost-effectiveness[1]. Additionally, the adaptation of chimeric antigen receptor (CAR) engineering technology provides a powerful means to enhance the therapeutic efficacy of allogeneic NK cells by improving their cancer-target specificity and anticancer activity[16]. As promising off-the-shelf CAR carriers, scalable NK lines[17], stem cell-derived differentiated NK cells[18–20] and cytokine-activated, blood-derived primary NK cells[16] have been explored extensively. Although substantial achievements in improving NK anticancer efficacy have been reported, CAR-NK production remains highly complex, laborious and time consuming, owing to its multistep processes including combinations of purification, expansion, activation and/or differentiation.

Recently, transcription factor (TF)-mediated direct-reprogramming strategies for the direct conversion of one type of differentiated cell into another have enabled the generation of various types of immune cell, such as dendritic cells[21], macrophages/macrophage-like cells[22] and HSPCs[23] from readily accessible cells. Here, we show that highly pure clinical-scale CD56^{bright}CD16^{bright} NK cells with or without CAR can be simply and easily generated through direct reprogramming without the need for time-, cost- and labour-intensive procedures such as differentiation and purification under feeder-free conditions. We also highlight that directly reprogrammed NK (drNK) cells are highly active and functional in terms

[1]Stem Cell Research Laboratory, Immunotherapy Research Center, Korea Research Institute of Bioscience and Biotechnology, Daejeon, Republic of Korea. [2]Department of Bioscience, KRIBB School, University of Science and Technology, Daejeon, Republic of Korea. ✉e-mail: june@kribb.re.kr

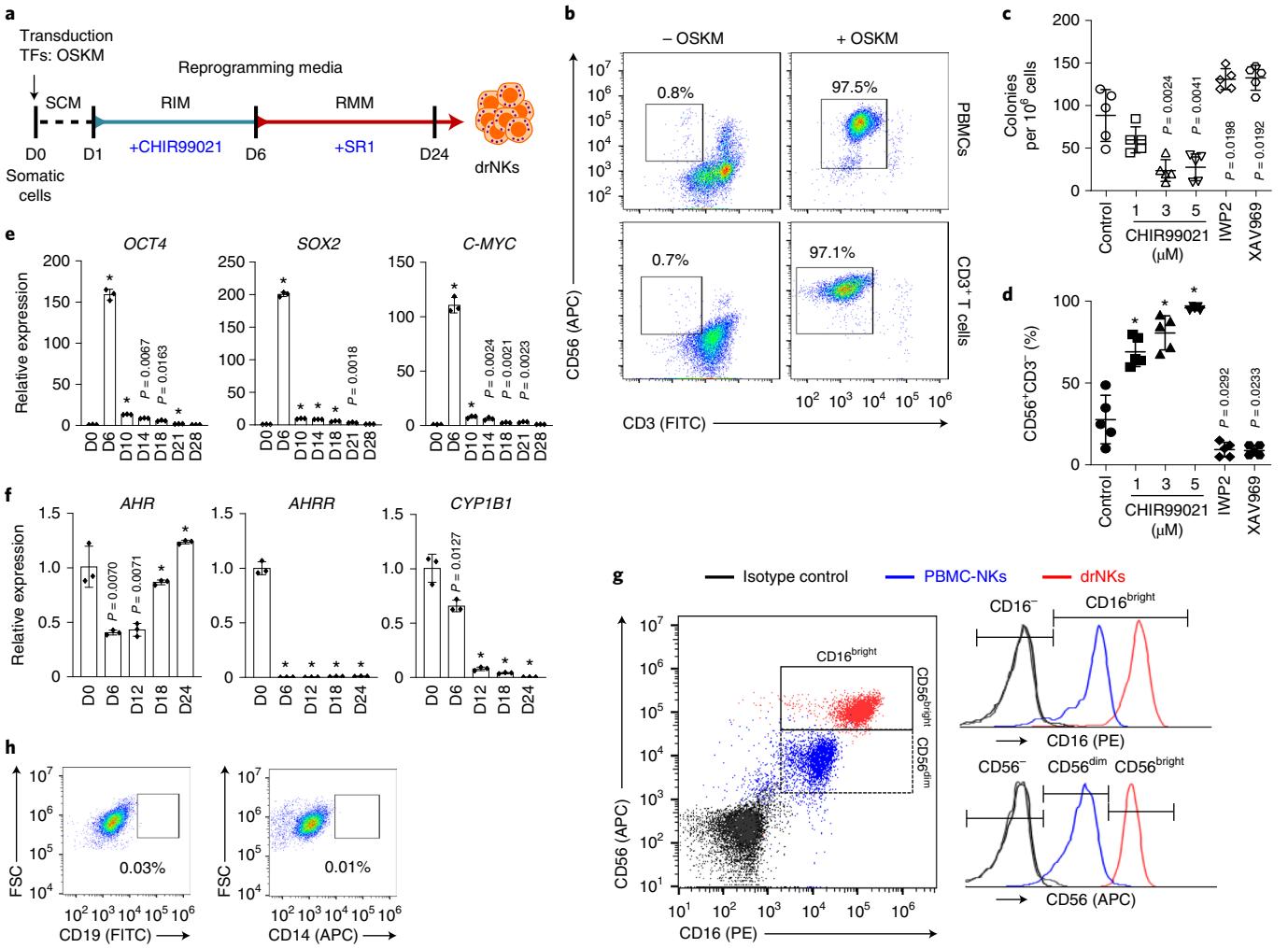

Fig. 1 | Generation of drNK cells by OSKM-mediated direct reprogramming. a, Schematic of direct drNK reprogramming. Starting cells (freshly isolated PBMCs or MACS-sorted CD3+ T cells) transduced with OSKM Sendai viruses in starting cell medium (SCM) were sequentially incubated with RIM containing 5 μM CHIR99021 and RMM containing 2 μM SR1 for the indicated number of days (D). TFs, transcription factors. **b**, Representative flow cytometry dot plots showing the induction of CD56+CD3− drNK cells from PBMCs or CD3+ T cells with or without OSKM transduction at day 24. **c**, Stimulatory effects of CHIR99021 on drNK reprogramming. A myeloid colony formation assay was performed on the OSKM-induced RICs generated with RIM in the presence of DMSO (control), 1, 3 or 5 μM CHIR99021, 2 μM IWP2 or 10 μM XAV969 for 5 d. The data represent means ± s.d. ($n = 5$). Statistical significance was determined by two-tailed Student's *t*-test (versus the DMSO control). **d**, Reprogramming efficiency of drNK from the RICs shown in **c**. The data represent means ± s.d. ($n = 5$ biological replicates per sample). Statistical significance was determined by two-tailed Student's *t*-test. *$P < 0.001$ (versus the DMSO control). **e**,**f**, RT-qPCR analysis of genes transcribing pluripotency transcription factors (*OCT4*, *SOX2* and *C-MYC*) (**e**) and AhR signalling-related genes (*AHR*, *AHRR* and *CYP1B1*) (**f**) at the indicated days of reprogramming from CD3+ T cells. The data represent means ± s.d. ($n = 3$). Statistical significance was determined by two-tailed Student's *t*-test. *$P < 0.001$ (versus the starting cells at day 0). **g**, Representative flow cytometry dot plots and histograms showing differential expression of surface CD56 and CD16 markers in 24-d drNK cells (red) and freshly isolated PBMC-NK cells (blue). **h**, Representative flow cytometry dot plots showing no induction of CD19+ B cells and CD14+ monocytes in 24-d drNK cells. For all of the flow cytometry experiments, appropriate isotype control monoclonal antibodies (black) were used to determine the level of background staining.

of their anticancer cytotoxicity and immunoregulatory activity, and thus may provide a promising alternative therapeutic method for ready-to-use NK cancer immunotherapy.

Results

Generation of drNK cells. In an attempt to obtain NK cells through direct reprogramming mediated by pluripotency transcription factors (Oct4, Sox2, Klf4 and c-Myc (OSKM)) (Fig. 1a), we focused on optimizing the NK fate-specific reprogramming medium (reprogramming initiation medium (RIM) and reprogramming maturation medium (RMM)) by screening for the beneficial effects of selected soluble factors (growth factors, cytokines and small molecules) known to be effective in NK lineage commitment and function. The NK reprogramming effects of various combinations of supplements and different starting cells, including freshly isolated peripheral blood mononuclear cells (PBMCs) and PBMC subsets (CD3+, CD3−, CD3−CD56−, CD14+, CD19+, CD34+, CD34−, CD34−CD56− and CD56− cells) were determined through a comparison of the percentage of CD56+CD3− cells, which represent the NK population. Importantly, among the tested factors, a combinatorial treatment with a Wnt signalling activator (CHIR99021, a GSK3β inhibitor) and an aryl hydrocarbon receptor (AhR) inhibitor (StemRegenin-1 (SR1)) was found to be most effective in the production of drNK cells (Fig. 1b and Supplementary Fig. 1a–d). OSKM-transduced PBMCs (96.1 ± 2.5% CD56+CD3−; 8,300 ± 4,529-fold increase in numbers per starting cell at reprogramming day 28; $n = 8$) or

PBMC-isolated CD3+ T cells (hereafter referred to as CD3+ T cells; 93.8 ± 5.6% CD56+CD3−; 5,280 ± 2,194-fold increase in numbers per starting cell at reprogramming day 28; $n = 5$) were most efficiently converted into CD56+CD3− cells after initial incubation with RIM (plus interleukin-3 (IL-3), IL-6, stem cell factor (SCF), fms-like tyrosine kinase 3 ligand (FLT3L) and thrombopoietin (TPO)) containing 5 μM CHIR99021 for 5 d and subsequent incubation with RMM (plus IL-2, IL-7, IL-15, SCF and FLT3L) containing 2 μM SR1 for more than 18 d (Fig. 1b and Supplementary Fig. 1a–d). Under the same conditions, drNK cells were also produced from other PBMC subsets (CD3−, CD3−CD56−, CD34+, CD34− and CD34−CD56− cells), but at different efficiency and yield (Supplementary Fig. 1e,f). Notably, our reprogramming conditions for drNK cells were not sufficient to convert CD19+ B cells or CD14+ monocytes into drNK cells (Supplementary Fig. 1e,f). The total cell numbers of PBMC-NK cells, CD19+ B cells and CD14+ monocytes were not substantially enhanced by the reprogramming process of the drNK cells (Supplementary Fig. 1g). The numbers of CD56+CD3− cells were slightly decreased in the reprogramming-cultured PBMC-NK population (Supplementary Fig. 1f), suggesting phenotypic changes of the original cells, possibly due to transduction and/or culture conditions during the early stages of reprogramming. The drNK cells derived from both unfrozen and frozen-thawed PBMCs could be maintained or expanded for more than six passages without significant loss of viability or proliferative ability (Supplementary Fig. 1h). Our results demonstrate that PBMCs and T cells, which have high availability and are easy to use, are an ideal starting cell choice for the production of drNK cells.

Stage-specific GSK3 and AhR inhibition for the efficient reprogramming of drNK cells. In particular, activation of canonical Wnt signalling by GSK3 inhibition (CHIR99021) is used to modulate HSPC function and differentiation[24], as well as reprogramming efficiency[25]. Methylcellulose colony formation assay revealed that, in the early stages of reprogramming, non-determinative OSKM-transduced cells yielded different types of reprogramming intermediate cells (RICs) depending on the Wnt signalling activity (Fig. 1c). CHIR99021 effectively promoted the enrichment of NK lineage-prone RICs by suppressing the induction of unfavourable lineage commitment of myeloid cells (colony-forming-unit granulocytes, erythrocytes, monocytes and megakaryocytes), whereas treatment with a Wnt inhibitor (either IWP2 or XAV969) led to opposite results (Fig. 1c). The inductive effect of CHIR99021 on NK lineage commitment was also confirmed by the increased expression of NK-related genes (*C-Kit* (*CD117*), *CD27*, *GATA3*, *TBX21* and *CCL5*) (Supplementary Fig. 2a) and yields of reprogrammed drNK cells (Fig. 1d). The beneficial effects of AhR antagonism with SR1 or silencing of AhR expression have been described in NK differentiation of CD34+ HSPCs[26], PSCs[27] and innate lymphoid cell type 3 subsets[28]. As another NK lineage-specifying cue, an AhR antagonist (either SR1 or CH223191) was found to be a potent stimulator of conversion of CHIR99021-enriched RICs to fully reprogrammed NK cells with high efficiency.

OSKM-transduced PBMCs (Supplementary Fig. 2b) or CD3+ T cells (Fig. 1e and Extended Data Fig. 1a–c) displayed early transient upregulation of pluripotency genes (*OCT4*, *SOX2* and *C-MYC*) as well as haematopoietic progenitor-related genes (*C-Kit* (*CD117*), *CD27, CD34*, *CD38*, *CD49* and/or *CD90*). Peak expression was observed on day 6 of reprogramming and was followed by upregulation of NK-related genes (*CD16*, *CD56*, *NKP46*, *NKP30* and/or *NKR*). In addition, downregulation of T cell-related genes (*CD3E*, *GATA3*, *HES1* and *TCF1*) after upregulation of pluripotency- and haematopoietic progenitor-related genes was found during reprogramming of CD3+ T cells (Extended Data Fig. 1c). As expected, the expression of pluripotency genes in the reprogramming intermediates of drNK cells was markedly lower than that in induced pluripotent stem cell (iPSC) reprogramming intermediates, whereas the expression of haematopoietic progenitor-related genes was higher (Supplementary Fig. 2c). Although upregulation of haematopoietic progenitor-related genes was observed, induction of CD34+ progenitor-like cells was not observed in fluorescence-activated cell sorting analysis (Supplementary Fig. 2d). After transient upregulation of pluripotency transcription factors, expression of the *AHR*, *AHRR* and *CYP1B1* genes was suppressed[29,30]; however, this suppression of *AHR*, but not *AHRR* and *CYP1B1*, was partially reversed during a later stage of reprogramming (Fig. 1f and Supplementary Fig. 2b). Collectively, our findings showed that stage-specific control of Wnt/β-catenin and AhR signalling is critical for efficient reprogramming of drNK cells.

Phenotypic characteristics of the drNK cells. According to flow cytometry of CD56 versus CD16, most drNK cells were double positive for CD56 and CD16 and negative for other lineage markers (CD19 (B cells) and CD14 (monocytes)) (Fig. 1g,h). Notably, all three populations of NK, 24-d drNK, fresh PBMC-NK and PSC-NK cells (embryonic stem cell-NK and iPSC-NK cells) differed phenotypically in their relative CD56 and CD16 expression (Fig. 1g and Supplementary Fig. 3a). By comparing CD56 and CD16 expression levels in freshly isolated PBMC-NK cells featured as $CD56^{dim}CD16^{bright}$ cells, we defined drNK cells as $CD56^{bright}CD16^{bright}$ cells (Fig. 1g). Notably, the level of CD16 expression in drNK cells was higher than that in PBMC-NK and PSC-NK cells (Fig. 1g and Supplementary Fig. 3a). We also found that most PBMC-NK cells cultured with drNK cell reprogramming medium showed higher expression of CD56, comparable to cytokine-activated PBMC-NK cells, but the numbers of CD16+ cells were markedly lower, thus resulting in greater heterogeneity (Supplementary Fig 3b).

Overall, comparative transcriptional and immunophenotypic profiling revealed a close phenotypic similarity between drNK and conventional NK cells (PBMC-NK, UCB-NK and PSC-NK cells (embryonic stem cell-NK and iPSC-NK cells)) but also some differences (Fig. 2 and Supplementary Fig. 3). A comparison of the genome-wide expression fold changes between drNK and PBMC-NK cells revealed a strong correlation (Pearson's correlation coefficient; $\gamma = 0.934–0.941$), thus indicating a high similarity at the molecular level (Fig. 2a). However, we also identified 1,523 differentially expressed genes (DEGs) ($P \leq 0.05$; $\log_2[\text{ratio}] \geq 1$), of which 1,054 were upregulated and 469 were downregulated in drNK cells compared with PBMC-NK cells (Supplementary Fig. 4a,b). Gene Ontology analysis indicated that these DEGs were mainly involved in the mitotic cell cycle and immune response, particularly NK-mediated cytotoxicity (Fig. 2b and Supplementary Fig. 4c,d). The upregulated DEGs included genes encoding NK activating receptors (*CD16A*, *CD16B*, *NKp30*, *KIR2DL4*, *KIR2DS5* and *CD59*), cytokine receptors (*IL2RB*, *IL2RG*, *IL4R*, *IL12RB2* and *IL18R1*), chemokine receptors (*CCR1*, *CCR2*, *CXCR3*, *CCR6*, *CX3CR1* and *CXCR3*), adhesion molecules (*NCAM1*, *ALCAM* and *ICAM3*) and MHC class II cell-surface receptors (*HLA-DRB1* and *HLA-DRA*) (Fig. 2b,c).

The cytotoxic and immunomodulatory effector functions of NK cells are regulated by a combination of activating and inhibitory NK receptors, natural cytotoxicity receptors (NCRs) and costimulatory receptors[31]. Immunophenotyping also revealed that drNKs, compared with NK cells from PBMCs, UCB and PSCs, overexpressed the major activating receptors CD16, CD69, NKG2D and DNAM-1 and the NCRs NKp44 and NKp46 (Fig. 2d,e). The expression of NKp30—another NCR in drNK cells—was similar to that observed in PSC-NK cells but relatively higher than that in PBMC-NK and UCB-NK cells (Fig. 2d,e). The drNK cells also substantially expressed the MHC class I-dependent inhibitory killer cell immunoglobulin-like receptors KIR2DL1, KIR2DL2/DL3 and KIR3DL1 (Fig. 2d,e), as well as the C-type lectin inhibitory

receptor CD94/NKG2A (Supplementary Fig. 4e), which are important for NK alloreactivity effects. Furthermore, analysis of T cell receptor gene rearrangements using a PCR-based *TCRB* gene clonality assay showed that reproducible distinct bands of the rearranged *TCRB* chain gene were not amplified from independent drNK cell sets derived from T cells (T-drNK cells 1, 2 and 3) and whole unsorted PBMCs (PBMC-drNK cells 1, 2 and 3), but one or two non-reproducible bands with a smeared background were visible (Supplementary Fig. 5a). In addition, we also confirmed that T cell receptor-αβ$^+$ (TCR-αβ$^+$) populations were markedly reduced during reprograming of T cells into drNK cells and were not redetected in fully reprogrammed drNK cells, as determined by the surface expression of TCR-αβ$^+$ (Supplementary Fig. 5b). Likewise, there were also no TCR-αβ$^+$ populations in PBMC-drNK cells. This indicates that drNK cells are non-clonal and derived from heterogeneous cell populations.

Anticancer effects of drNK cells in vitro. Next, we assessed the functional capabilities of drNK cells by determining their ability to induce cytolytic activity, cytokine secretion and degranulation. Notably, even at low effector-to-target (E:T) ratios without stimulation, drNK cells exhibited high cytolytic activity against a broad range of haematological and solid cancer cells in vitro, including: brain (SK-N-BE and U373MG), blood (K562 and THP1), breast (MCF-7 and SK-BR-3), colon (HCT116, SW480 and SW620), liver (Hep3B and HepG2), lung (A549 and NCI-H460), ovarian (SK-OV-3), pancreatic (MIA PaCa-2) and prostate (DU145, LNCap and PC-3) (Fig. 3a,b). Importantly, their cytolytic activity and secretion of cytokines (IFN-γ and TNF-α) and granzyme B in response to blood (K562; Extended Data Fig. 2a,c), colon (HCT116, SW480 and SW620; Fig. 3b,c) and liver (HepG2) cancer cells (Extended Data Fig. 2b) were greater than those of PBMC-NK and UCB-NK cells. Similarly, drNK cells displayed more CD107a degranulation than PBMC-NK cells after stimulation with colon cancer cells (HCT116, SW480 and SW620) (Fig. 3d,e). These results suggest that drNK cells have a strong ability to kill a wide variety of cancer cells.

Anti-CSC effects of drNK cells. Three-dimensional (3D) in vivo-like CD133$^+$ CSC-enriched SW620 spheroids (CD133$^+$ SW620 cells) were prepared from parental SW620 colon cancer cells (SW620) via a modified 3D spheroid culture method (Fig. 4a,b)[32] to assess the anti-CSC activity of drNK cells. Compared with their parental SW620 cells, drNK cells more effectively killed the CD133$^+$ SW620 cells, even at E:T ratios as low as 0.25:1 and 1:1 (Fig. 4c,d). In addition, the ability of drNK cells to degranulate CD107a and secrete granzyme B and cytokines (IFN-γ and TNF-α) was greater against the CD133$^+$ SW620 cells than the parental SW620 cells (Fig. 4e,f). Because the infiltration capability of NK cells is associated with better anticancer effects and prognosis in solid cancers, including colon cancer[33], we further monitored the integrity of the CD133$^+$ SW620 cells fluorescently labelled with green fluorescent protein (GFP) (CD133$^+$GFP$^+$ SW620 cells) for NK infiltration and cytolytic activity, using bright-field and fluorescence microscopy. After drNK cell coculture for 24 h, the CD56$^+$ drNK cells (red dots) spontaneously infiltrated and interspersed with the CD133$^+$ SW620/GFP spheroids (Fig. 4g). Notably, whereas the CD133$^+$ SW620 cells cultured in the absence of drNK cells were homogeneously GFP positive, the integrity of the tight spheroid border in the CD133$^+$ SW620 cells and the overall number of GFP$^+$ cells significantly decreased concomitantly with a significant increase in CD107a after coincubation with drNK cells, thus indicating drNK cell-mediated CSC elimination (Fig. 4g,h). To further assess the anti-CSC activity of drNK cells in vivo, we injected mice subcutaneously with GFP-SW620 cells and then injected them intravenously with drNK cells. The drNK cell treatment significantly eliminated the CD133$^+$ CSCs in SW620-induced tumours in vivo (Fig. 4i). This drNK cell-mediated anti-CSC effect was further supported by the significantly lower colony formation ability of tumour cells isolated from the SW620 xenografts injected with drNK cells compared with controls injected with phosphate buffered saline (PBS) (Fig. 4j). These results suggest that drNK cells effectively target and kill both bulk colon cancer cells and CSCs in vitro and in vivo.

Antibody-dependent cell-mediated cytotoxicity (ADCC) of drNK cells. Because the Fc receptor CD16 is highly abundant on drNK cells, we next performed artificial in vitro ADCC activation assays using the anti-CD20 IgG1 rituximab and an agonistic anti-human κ light chain (KLC) antibody in the absence of target cells to determine the correlation between CD16 expression and ADCC functional capability (Fig. 5a). Consistent with phenotypic observations, we found that after CD16 engagement with rituximab, cross-linking of the rituximab bound on the NK cells with anti-KLC antibody more effectively improved CD16-mediated ADCC in drNK cells than in PBMC-NK cells, as demonstrated by greater expression of indicators of NK activation and ADCC activity, such as CD107a (Fig. 5b), IFN-γ, CCL3 and CCL4 (Fig. 5c). At the molecular level, we also confirmed that drNK and PBMC-NK cells exhibited differential activation of the downstream members of the PI3K/AKT and MAPK/ERK pathways in CD16-dependent NK activation[34,35] (Fig. 5d,e). Treatment with agonistic anti-KLC antibody after CD16 engagement with rituximab more effectively increased the phospho-AKT (pAKT) and phospho-ERK (pERK) abundance in drNK cells than in PBMC-NK cells (Fig. 5d). These results suggest that CD16-dependent activation of PI3K/AKT and ERK signalling pathways is associated with enhanced ADCC activity of drNK cells. We further examined the functional ability of drNK cells to kill therapeutic antibody-coated cancer cells via ADCC activity. The Food and Drug Administration-approved anti-epidermal growth factor receptor (anti-EGFR) IgG1 cetuximab has been demonstrated to be effective in the treatment of EGFR-expressing, metastatic colorectal cancers[36] and has also shown promise in combination with other anticancer therapeutics such as NK cells[37]. The ADCC of drNK cells was compared in low- (SW620) and high-EGFR-expressing colon cancer cells (HCT116 and SW480) (Fig. 5f). Exposure of drNK cells to the cetuximab-coated HCT116 and SW480 cells, but not to SW620

Fig. 2 | Phenotypic properties of drNK cells. a–c, Microarray-based comparative analysis of gene expression between drNK cells and PBMC-NK cells. **a**, Pearson correlations between pairwise comparisons using the median values of gene expression for each cell type (PBMC-NK 1, PBMC-NK 2, drNK 1 and drNK 2). Top right: Pearson correlation values of the genes with more than ten counts per million reads. Bottom left: scatter plot data of the $\log_2$[counts per million reads]. Middle: histograms of the log[counts per million] for each sample. **b**, Major DEGs in drNK cells. The data are presented as fold changes relative to control levels (PBMC-NK cells). **c**, RT-qPCR confirmation of some of the DEGs shown in **b**. The data represent means ± s.d. ($n = 3$ biological replicates for each sample). Statistical significance was determined by two-tailed Student's *t*-test. **d**, Representative flow cytometry histogram plots showing the expression patterns of activating receptors (CD16, CD69, NKG2D and DNAM-I), NCRs (NKp30, NKp44 and NKp46) and inhibitory receptors (KIR2DL1, KIR2DL2 and KIR3DL1) in drNK (red), PBMC-NK (black), UCB-NK (dark blue), embryonic stem cell-NK (ESC-NK; green) and iPSC-NK cells (orange). Isotype control monoclonal antibody (mAb) (light blue) was used to determine the level of background staining. **e**, Quantitative graph of the results shown in **d**. The data represent means ± s.d. ($n = 3$–11 biological replicates for each sample). Statistical significance was determined by two-tailed Student's *t*-test. *$P < 0.001$ (versus drNK cells).

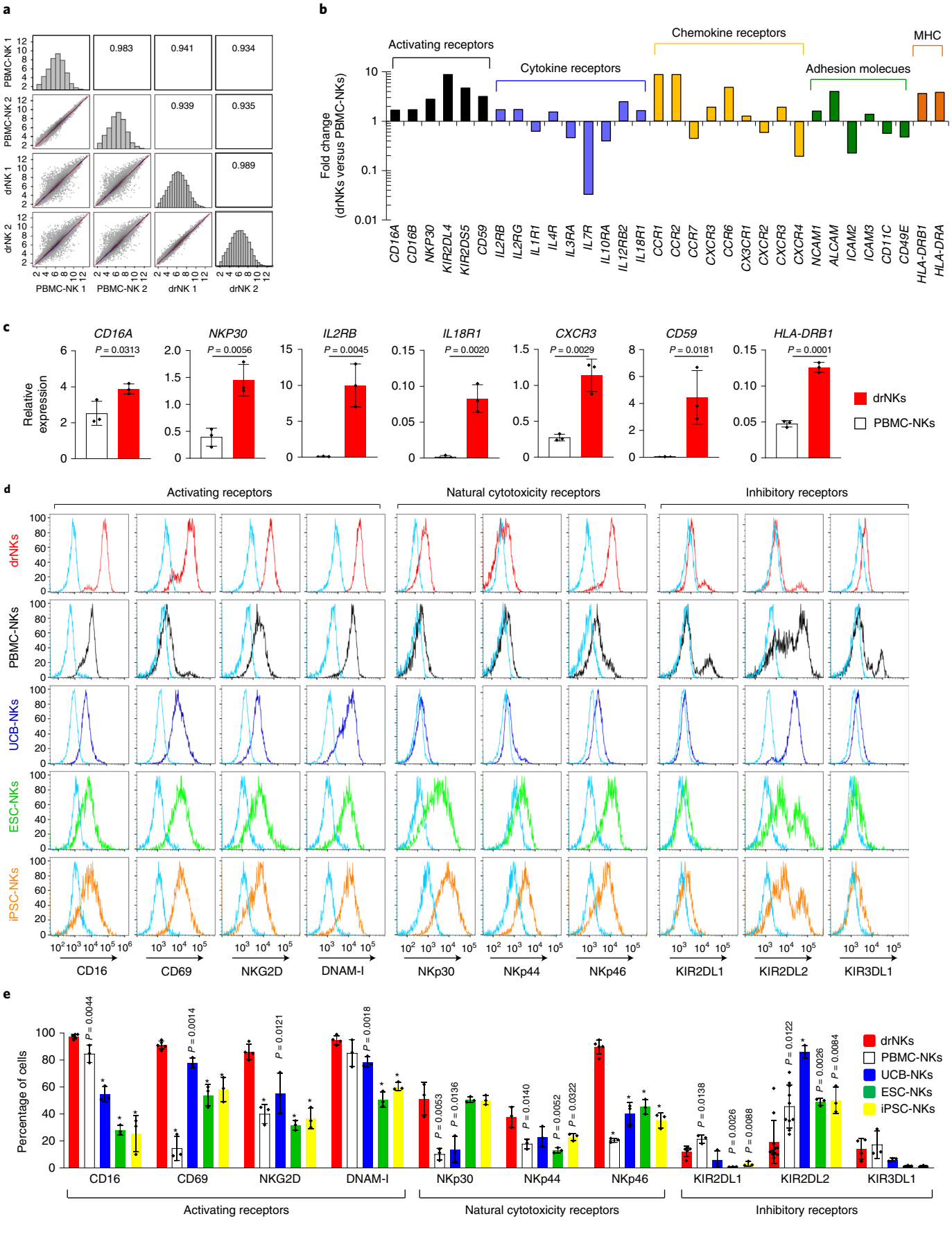
a
PBMC-NK 1
PBMC-NK 2
drNK 1
drNK 2
0.983
0.941
0.934
0.939
0.935
0.989
b
Activating receptors
Cytokine receptors
Chemokine receptors
Adhesion molecues
MHC
Fold change (drNKs versus PBMC-NKs)
CD16A CD16B NKP30 KIR2DL4 KIR2DS5 CD59 IL2RB IL2RG IL1R1 IL4R IL3RA IL7R IL10RA IL12RB2 IL18R1 CCR1 CCR2 CCR7 CXCR3 CCR6 CX3CR1 CXCR2 CXCR3 CXCR4 NCAM1 ALCAM ICAM2 ICAM3 CD11C CD49E HLA-DRB1 HLA-DRA
c
CD16A P = 0.0313
NKP30 P = 0.0056
IL2RB P = 0.0045
IL18R1 P = 0.0020
CXCR3 P = 0.0029
CD59 P = 0.0181
HLA-DRB1 P = 0.0001
Relative expression
drNKs
PBMC-NKs
d
Activating receptors
Natural cytotoxicity receptors
Inhibitory receptors
drNKs
PBMC-NKs
UCB-NKs
ESC-NKs
iPSC-NKs
CD16 CD69 NKG2D DNAM-I NKp30 NKp44 NKp46 KIR2DL1 KIR2DL2 KIR3DL1
e
Percentage of cells
P = 0.0044 P = 0.0014 P = 0.0121 P = 0.0018 P = 0.0053 P = 0.0136 P = 0.0140 P = 0.0052 P = 0.0322 P = 0.0138 P = 0.0026 P = 0.0088 P = 0.0122 P = 0.0026 P = 0.0084
drNKs
PBMC-NKs
UCB-NKs
ESC-NKs
iPSC-NKs
CD16 CD69 NKG2D DNAM-I NKp30 NKp44 NKp46 KIR2DL1 KIR2DL2 KIR3DL1
Activating receptors
Natural cytotoxicity receptors
Inhibitory receptors

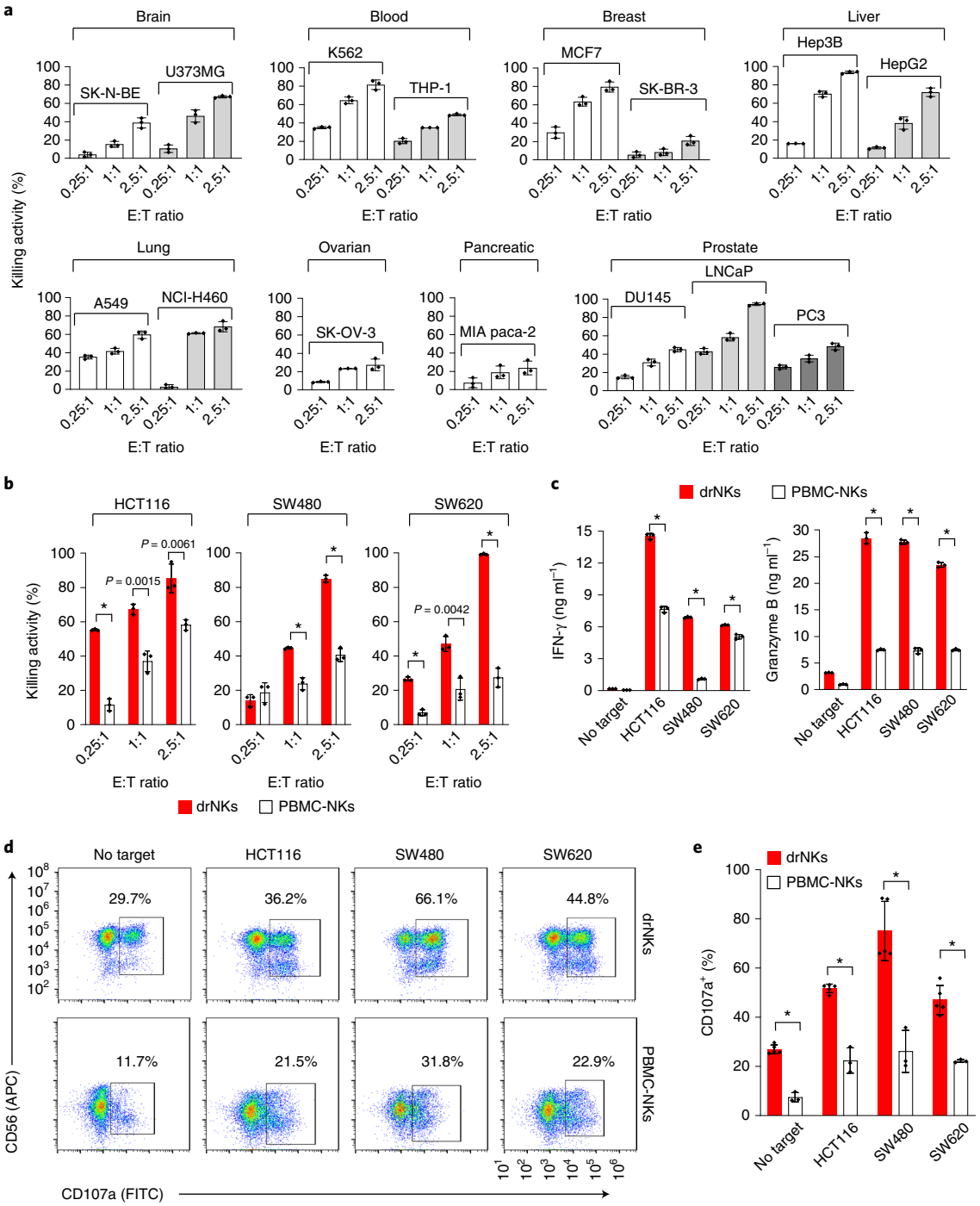

Fig. 3 | Functional properties of drNK cells. a, Cytolytic activity of drNK cells against a wide range of cancers, measured with a calcein-release assay. The data represent means ± s.d. ($n = 3$). **b**, Comparisons of the cytolytic activity of drNK and PBMC-NK cells. drNK cells or PBMC-NK cells were cocultured with the indicated colon cancer cells for 4 h at E:T ratios of 0.25:1, 1:1 or 2.5:1. The cytolytic activity was measured with a calcein-release assay. The data represent means ± s.d. ($n = 3$ biological replicates for each sample). Statistical significance was determined by two-tailed Student's *t*-test. *$P < 0.001$ (versus drNK cells). **c**, Comparison of the IFN-γ and granzyme B secretion of drNK and PBMC-NK cells. drNK cells or PBMC-NK cells were cocultured with medium alone (no target) or with the indicated colon cancer cells at an E:T ratio of 1:1. IFN-γ and granzyme B release were determined by ELISAs in culture supernatants harvested 16 h after stimulation with medium or cancer cells. The data represent means ± s.d. ($n = 3$ biological replicates for each sample). Statistical significance was determined by two-tailed Student's *t*-test. *$P < 0.001$ (versus drNK cells). **d**, Comparison of the CD107a expression frequency on drNK cells and PBMC-NK cells. drNK cells or PBMC-NK cells were cocultured with medium alone or with the indicated colon cancer cells for 16 h at an E:T ratio of 1:1. Then, the percentage of $CD107a^+$ cells was measured by flow cytometry. A negative isotype control was used to determine the level of background staining. **e**, Quantitative graph of the results shown in **d**. The data represent means ± s.d. ($n = 3$–5 biological replicates for each sample). Statistical significance was determined by two-tailed Student's *t*-test. *$P < 0.001$ (versus drNK cells).

cells, significantly elevated the frequency of IFN-γ-producing drNK cells relative to uncoated cells (Fig. 5g). In agreement with this finding, the cytolytic activity of drNK cells was significantly enhanced against the cetuximab-coated HCT116 and SW480 cells but not SW620 cells (Fig. 5h), thus suggesting that the drNK cell-mediated ADCC against the cetuximab-coated colon cancer

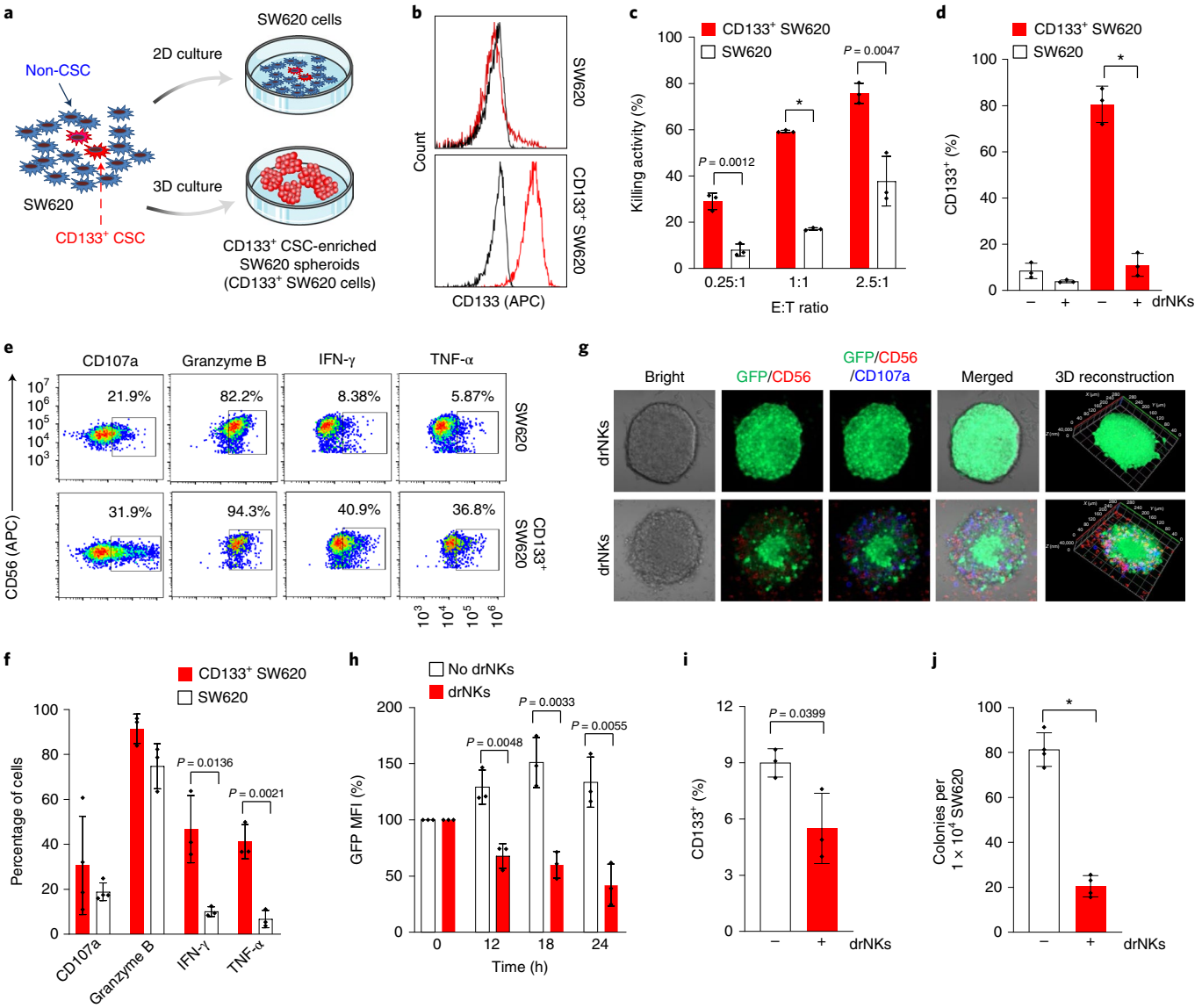

Fig. 4 | CSC killing activity of drNK cells. a, Schematic showing the preparation of SW620 2D controls (SW620 cells) and CD133+ CSC-enriching 3D spheroids (CD133+ SW620 cells). **b**–**h**, Anti-CSC activity of drNK cells in vitro. **b**, The percentages of CD133+ CSCs in SW620 and CD133+ SW620 (red) cells were measured by flow cytometry analysis. An isotype control mAb (black) was used to determine the level of background staining. **c**,**d**, Preferential killing of CD133+ CSCs by drNK cells. **c**, Comparison of the cytolytic activity of drNK cells against SW620 and CD133+ SW620 cells. The drNK cells were cocultured with control SW620 or CD133+ SW620 cells for 2 h at E:T ratios of 0.25:1, 1:1 or 2.5:1. The cytolytic activity was measured with a calcein-release assay. The data represent means ± s.d. ($n = 3$ biological replicates for each sample). Statistical significance was determined by two-tailed Student's *t*-test. *$P < 0.001$ (versus SW620 cells). **d**, Percentages of CD133+ CSCs after the drNK cell coculture shown in **c**. An E:T ratio of 1:1 was used. The data represent means ± s.d. ($n = 3$ biological replicates for each sample). Statistical significance was determined by two-tailed Student's *t*-test. *$P < 0.001$ (versus no drNK cells). **e**, Representative flow cytometry dot plots showing comparisons of the cytokine secretion of drNK cells in response to the SW620 and CD133+ SW620 cells shown in **c**. An E:T ratio of 1:1 was used. After coculture, the percentages of IFN-γ+, TNF-α+, granzyme B+ or CD107a+ drNK cells were measured by flow cytometry analysis. A negative isotype control was used to determine the level of background staining. **f**, Quantitative graph of the results shown in **e**. The data represent means ± s.d. ($n = 3$ biological replicates for each sample). Statistical significance was determined by two-tailed Student's *t*-test (versus SW620). **g**, Representative confocal microscopy images showing the GFP+ SW620 frequency (green) in 3D spheroids. CD133+ SW620-GFP spheroids were infiltrated with or without drNK cells for 3 h at an E:T ratio of 1:1. Immunofluorescence was performed with anti-CD56 (red) and anti-CD107a (blue). **h**, Quantitative analysis of the spheroid GFP intensity obtained by time-lapse microscopy at the indicated times. The cytotoxicity of drNK cells against CD133+ SW620-GFP spheroids was assessed by the mean fluorescence intensity (MFI) of GFP. The data represent means ± s.d. ($n = 3$ biological replicates for each sample). Statistical significance was determined by two-tailed Student's *t*-test (versus no drNKs). **i**,**j**, Anti-CSC activity of drNK cells in SW620 xenograft models. **i**, Decreased frequency of CD133+ CSCs after drNK cell treatment. Tumour tissues were extracted from mice that had received SW620 cancer xenografts injected with control PBS (no drNK cells) or drNK cells and dissociated into single cells. The percentages of CD133+ CSCs were measured by flow cytometry analysis. The data represent means ± s.d. ($n = 3$ biological replicates for each sample). Statistical significance was determined by two-tailed Student's *t*-test (versus no drNKs). **j**, Colony-forming unit assays of SW620 cancer xenografts were performed by culturing single cells from the tumour tissues shown in **i**. The numbers of colonies were counted after 10 d of culture. The data represent means ± s.d. ($n = 4$ biological replicates for each sample). Statistical significance was determined by two-tailed Student's *t*-test. *$P < 0.001$ (versus no drNK cells).

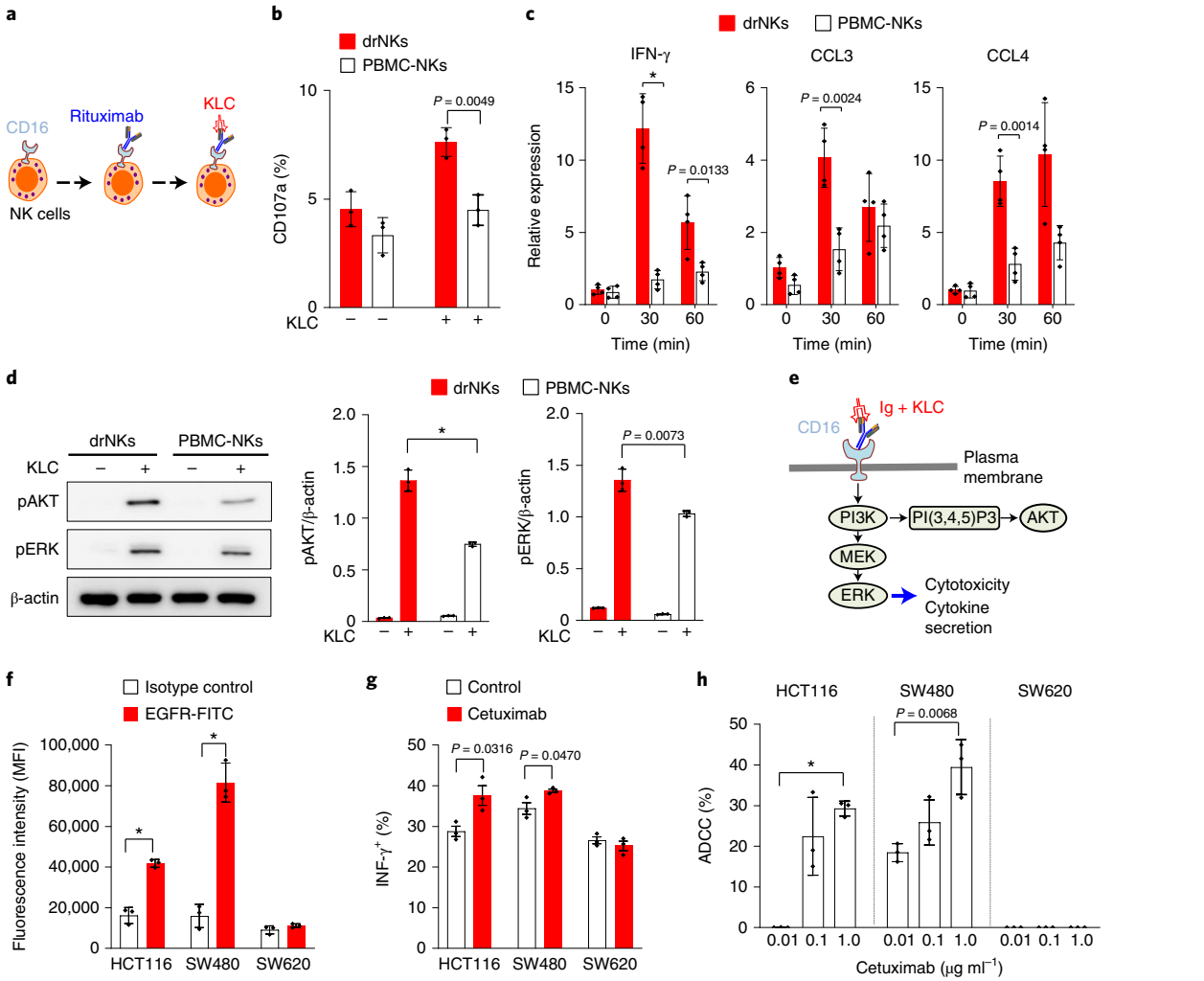

Fig. 5 | ADCC activity of drNK cells. a, Schematic of an artificial in vitro ADCC assay. **b**, Percentage of CD107a$^+$ cells measured by flow cytometry analysis. drNK cells or PBMC-NK cells pre-incubated with rituximab were incubated with or without anti-human KLC for 4 h at 37 °C. The data represent means ± s.d. ($n = 3$). Statistical significance was determined by two-tailed Student's *t*-test. (versus drNKs). **c**, RT-qPCR analysis of the cytokine IFN-γ and the chemokines CCL3 and CCL4 at the indicated times of KLC-treatment in drNK cells or PBMC-NK cells. The data represent means ± s.d. ($n = 3$ biological replicates for each sample). Statistical significance was determined by two-tailed Student's *t*-test. *$P < 0.001$ (versus drNK cells). **d**, Representative western blot (left) and semi-quantitative graph (right) for pAKT and pERK1/2. drNK or PBMC-NK cells were treated with KLC for 2 min after pre-incubation with rituximab. Cell lysates were then immunoblotted with antibodies to pAKT or pERK. The data represent means ± s.d. ($n = 3$ biological replicates for each sample). Statistical significance was determined by two-tailed Student's *t*-test. *$P < 0.001$ (versus drNKs). **e**, Schematic of the events of FcγRIIIa signalling in NK cells. **f**, Cell-surface expression of EGFR, as determined by flow cytometry analysis of colon cancer cells (HCT116, SW480 and SW620). The data represent means ± s.d. ($n = 3$ biological replicates for each sample). two-tailed Student's *t*-test. *$P < 0.001$ (versus isotype control). **g**, IFN-γ expression frequency on drNK cells in response to cetuximab-coated colon cancer cells. drNK cells were stimulated with the indicated colon cancer cells with or without 0.1 μg ml^{-1} cetuximab (EGFR monoclonal antibody) pre-coating for 2 h at an E:T ratio of 1:1. The percentage of IFN-γ$^+$ drNK cells was measured by flow cytometry. The data represent means ± s.d. ($n = 3$ biological replicates for each sample). Statistical significance was determined by two-tailed Student's *t*-test (versus no cetuximab control). **h**, ADCC of drNK cells against cetuximab-coated colon cancer cells. drNK cells were incubated with the indicated cetuximab-coated colon cancer cells for 2 h at an E:T ratio of 1:1. The cytolytic activity was measured by a calcein-release assay. The data represent means ± s.d. ($n = 3$ biological replicates for each sample). Statistical significance was determined by two-tailed Student's *t*-test. *$P < 0.001$ (versus control).

cells was positively correlated with EGFR expression. These findings strongly indicated that drNK cells are highly potent effector cells with ADCC, and that their ADCC activity ultimately contributes to overcoming inhibitory signals and specifically killing cancer cells without causing notable adverse effects.

Adaptive properties of drNK cells. Next, we explored the adaptive immunological properties of drNK cells by evaluating their ability to induce a memory-like response and their immunomodulatory effects on adaptive immune cells. drNK cells preactivated with cytokines (IL-12 + IL-5 + IL-18) for 16 h were allowed to rest for 1 week to induce antigen-unspecific, memory-like responses (Fig. 6a)[38,39]. Importantly, after restimulation with either cytokines (IL-12 + IL-15) or K562 cancer cells, the cytokine-preactivated drNK cells displayed an enhanced ability to produce IFN-γ (Fig. 6b,c) and to kill K562 cancer cells (Fig. 6d). These findings suggest that cytokine priming alone can convert drNK cells to more potent drNK cells with adaptive memory-like properties.

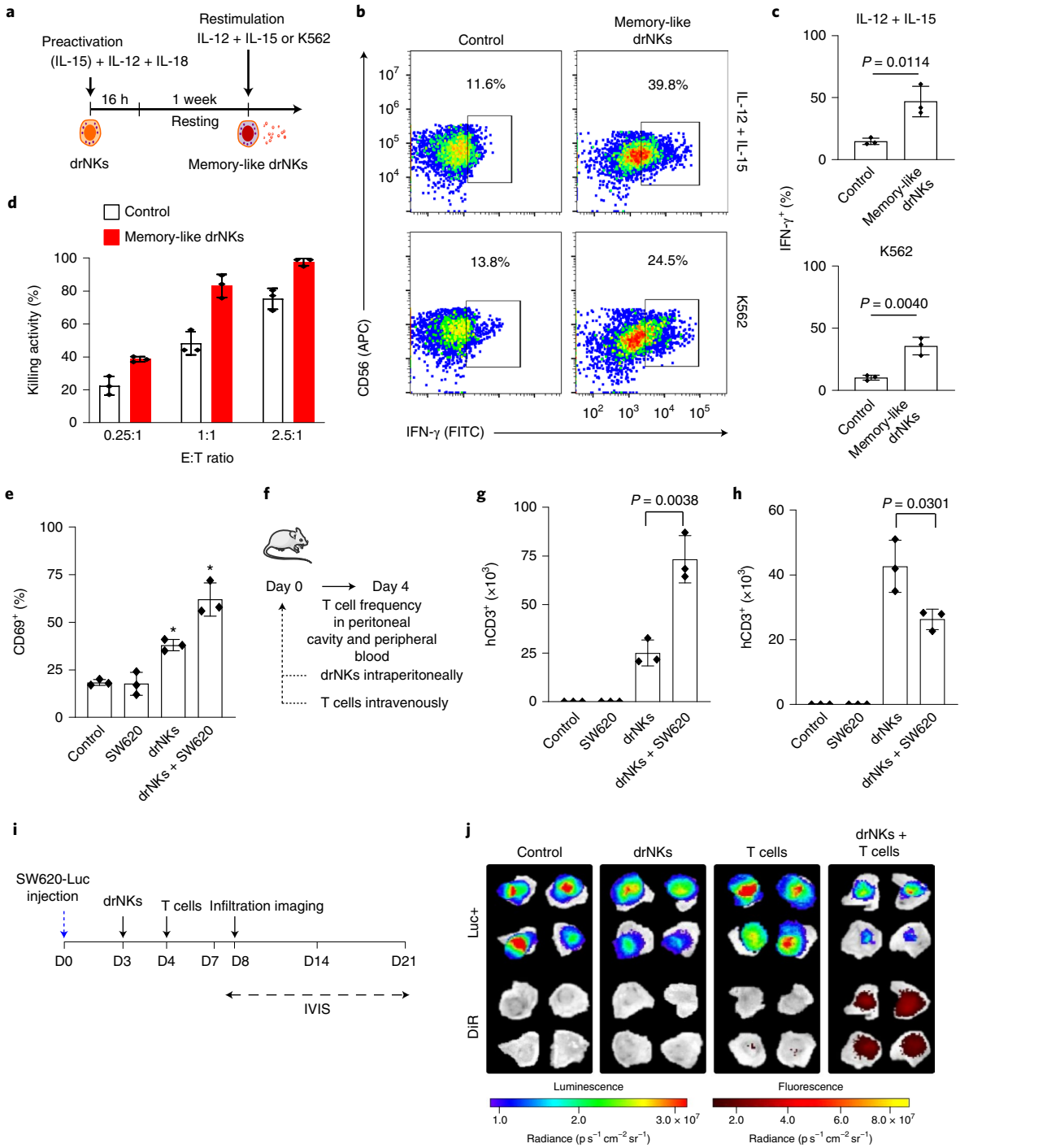

Fig. 6 | Adaptive properties of drNK cells. a, Experimental design of the induction of cytokine-induced memory-like drNK cells. **b**, Enhanced IFN-γ expression frequency on memory-like drNK cells restimulated with either cytokines or K562 cancer cells. **c**, Quantitative graph of the results shown in **b**. The data represent means ± s.d. ($n = 3$). Statistical significance was determined by two-tailed Student's *t*-test (versus control). **d**, Enhanced cytolytic activity of memory-like drNK cells. Control drNK cells or memory-like drNK cells were cocultured with K562 cancer cells for 4 h at E:T ratios of 0.25:1, 1:1 or 2.5:1. The cytolytic activity was measured with a calcein-release assay. The data represent means ± s.d. ($n = 3$). Statistical significance was determined by two-tailed Student's *t*-test (versus control). **e**, T cell activation by drNK cells. $CD3^+$ T cells were treated with the indicated conditioned medium from a single culture, conditioned medium from cocultured drNK and SW620 cells or control medium for 16 h. The percentage of $CD69^+$ T cells was measured by flow cytometry analysis. The data represent means ± s.d. ($n = 3$ biological replicates for each sample). Statistical significance was determined by two-tailed Student's *t*-test. $^*P < 0.001$ (versus control). **f**–**h**, drNK-mediated T cell recruitment. Mice were injected intravenously with T cells and intraperitoneally with either control PBS or drNK cells (**f**). After 4 d, the frequency of human T cells in the peritoneal cavity (**g**) and peripheral blood (**h**) was measured. The data represent means ± s.d. ($n = 3$ biological replicates per sample). Statistical significance was determined by two-tailed Student's *t*-test. **i**, Schematic of an in vivo anticancer activity assay of T cells recruited by drNK cells. The mice injected subcutaneously with SW620-Luc cells were injected intravenously with PBS, drNK cells, activated T cells or drNK cells plus activated T cells on day 4. **j**, The infiltration of T cells in tumour xenografts was analysed through both bioluminescence (tumour xenograft) and fluorescence (DiR T cells) 5 d after injection with drNK cells or PBS control.

Because drNK cells showed high secretion of immunomodulatory cytokines such as IFN-γ and TNF-α (Fig. 3c and Extended Data Fig. 2c), we examined the effects of NK cell-released soluble factors on T cell responses. After incubation of $CD3^+$ T cells with conditioned medium from single cultures of SW620 cells (SW620-CM) and drNK cells (drNK-CM) and from cocultures of SW620 cells and drNK cells (drNK–SW620-CM), we assessed the resulting T cell activation by determining the percentages of $CD69^+$ (activation marker) T cells. T cell activation significantly increased after exposure to drNK-CM and further increased after exposure to SW620 cancer cell-stimulated drNK-CM, compared with the responses of the no-cell conditioned medium and SW620-CM groups (Fig. 6e), thus suggesting that soluble factors secreted from drNK cells are highly effective in T cell activation. Moreover, a T cell recruitment assay in vivo showed that the mice injected intravenously with drNK cell-activated T cells in vitro and intraperitoneally with drNK cells on the same day showed a higher T cell frequency in the peritoneal cavity and a lower T cell frequency in the peripheral blood than control mice injected with T cells alone (Fig. 6f–h), thus suggesting that NK cells also modulate T cell recruitment.

To further assess the actual effects of drNK cell-induced chemokines on T cell recruitment into tumour tissues in vivo, we transplanted in vitro-activated PBMC T cells labelled with a lipophilic near-infrared fluorescent dye DiR into SW620-Luc colon cancer-bearing mice and evaluated their homing to subcutaneous tumours (Fig. 6i). Remarkably, DiR fluorescence images of tumours (at day 8) revealed that the recruitment of DiR-labelled T cells to the tumour sites was enhanced by drNK cell co-injection (Fig. 6j). In further support of these findings, quantitative PCR with reverse transcription (RT-qPCR) analysis of tumour specimens showed that expression of the T cell marker gene *CD3D* was significantly higher in T cell and drNK cell co-injected groups than in untreated and drNK cell or T cell single-treated groups (Extended Data Fig. 3a). In accordance with these findings, the expression of chemokines such as CCL3, CCL4, CCL5 and IFN-γ was also upregulated in the T cell and drNK cell co-injected groups compared with the untreated and drNK cell or T cell single-treated groups (Extended Data Fig. 3b), thus indirectly suggesting the involvement of drNK cell-secreted chemokines in T cell recruitment into tumours. Overall, the results indicate that drNK cells effectively elicit adaptive immunity by modulating adaptive immune effector cells such as T cells in vitro and in vivo.

CAR-drNK cell generation by reprogramming. CAR engineering technology, which enables redirection of NK cytotoxicity and specificity, has drawn increasing attention as a promising tool with which to generate superior anticancer NK cells; however, a more efficient and simple CAR-NK manufacturing process for clinical applications is highly desirable. In our approach, we generated CAR-expressing drNK (CAR-drNK) cells by merging the OSKM reprogramming culture and CAR transfer. For CAR-drNK cell generation, second-generation CARs consisting of HER2- or CD19-specific scFv associated with a CD8 hinge and the transmembrane and intracellular domains of CD28 and CD3ζ in sequence (Fig. 7a) were constructed into an internal ribosome entry site (IRES)-GFP lentiviral vector. With the same drNK reprogramming protocol (Fig. 7b), we generated HER2-expressing drNK cells (HER2-CAR drNK cells) ($CD56^+CD3^-HER2\text{-}CAR^+$; 35.5 ± 3.0%) and CD19-expressing drNK cells (CD19-CAR drNK cells) ($CD56^+CD3^-CD19\text{-}CAR^+$; 31.4 ± 3.8%) through serial transduction with reprogramming transcription factors (at day 1) and CARs (HER2- and CD19-specific CAR constructs (Fig. 7a)) (at day 4) (Fig. 7c). The percentages of total $CD56^+CD3^-$ drNK cells (HER2-CAR drNK cells = 98.4 ± 0.8%; CD19-CAR drNK cells = 98.5 ± 0.9%) (Fig. 7c) were similar to those generated under CAR-untransfected reprogramming conditions (Fig. 1b). The phenotypic characteristics of the CAR-drNK cells showed that these cells retained a typical drNK cell phenotype characterized by high levels of CD56 and CD16 (Fig. 7c,d), high levels of the activating receptors CD69, NKG2D and DNAM-1, high levels of the NCRs NKp44 and NKp46 and low levels of inhibitory KIRs (Fig. 7d).

The enhanced functionality of CAR-drNK cells was confirmed without additional selection or purification. Compared with non-CAR drNK cells, the HER2-CAR drNK cells displayed enhanced cytolytic activity against the $HER2^+$ cancer cell lines COLO 205 (colon) and SK-OV-3 (ovarian), whereas no major changes in cytolytic activity between the non-CAR and HER2-CAR drNK cells were observed against $HER2^-$K562 cells (Fig. 7e,f). After cancer cell stimulation, the HER2-CAR drNK cells displayed higher CD107a expression than non-CAR drNK cells (Fig. 7g). The induction of CD107a expression was more pronounced after stimulation with $HER2^+$ COLO 205 and SK-OV-3 cells than $HER2^-$K562 cells (Fig. 7g). Likewise, compared with non-CAR drNK cells, CD19-CAR drNK cells were more effective in killing CD19-presenting B lymphoma cells (Raji B, SNU-291 and SNU-817) (Fig. 7h,i) and enhancing CD107a expression (Fig. 7j). These results clearly indicate that direct reprogramming generates target-specific CAR-drNK cells and that the introduction of cancer antigen-specific CARs confers specific and powerful anticancer activity against target cancer cells on drNK cells.

Fig. 7 | A simple alternative route for CAR-NK production. a, Schematic of the HER2- and CD19-CAR constructs. ID, intracellular domain; TM, transmembrane domain. **b**, Schematic of the reprogramming of direct CAR-drNK cells. **c**, Representative flow cytometry dot plots showing the induction of HER2-drNK (left) and CD19-drNK cells (right). **d**, Representative flow cytometry histogram plots showing the expression patterns of the NK receptors CD16, CD69, NKG2D, DNAM-I, NKp30, NKp44, NKp46, KIR2DL1, KIR2DL2 and KIR3DL1 in HER2-drNK cells. Isotype control mAb (light blue) was used to determine the level of background staining. The numbers indicate the amount of positive staining compared with isotype controls. **e**, Cell-surface expression levels of HER2 against various cancer cells (K562, COLO 205 and SK-OV-3), as measured by flow cytometry. The numbers indicate the amount of positive staining compared with isotype controls. **f**, Augmented cytolytic activity of HER2-drNK cells. drNK or HER2-drNK cells were cocultured with the indicated cancer cells for 4 h at E:T ratios of 0.25:1, 1:1 or 2.5:1. The cytolytic activity was measured by calcein-release assay. The data represent means ± s.d. ($n = 3$ biological replicates per sample). Statistical significance was determined by two-tailed Student's *t*-test (versus drNKs). **g**, Enhanced CD107a expression frequency on HER2-drNK cells. drNK or HER2-NK cells were cocultured with medium alone or with the indicated cancer cells for 4 h at an E:T ratio of 1:1. The percentage of $CD107a^+$ cells was measured by flow cytometry. The data represent means ± s.d. ($n = 3$ biological replicates for each sample). Statistical significance was determined by two-tailed Student's *t*-test (versus drNKs). **h**, Cell-surface expression levels of CD19 against B lymphoma cells (Raji B, SNU-291 and SNU-817), as measured by flow cytometry analysis. The numbers indicate the amount of positive staining compared with isotype controls. **i**, Augmented cytolytic activity of CD19-drNK cells. drNK or CD19-drNK cells were cocultured with the indicated B lymphoma cells for 4 h at E:T ratios of 0.25:1, 1:1 or 2.5:1. The cytolytic activity was measured by a calcein-release assay. The data represent means ± s.d. ($n = 3$ biological replicates for each sample). Statistical significance was determined by two-tailed Student's *t*-test. $^*P < 0.001$ (versus drNKs). **j**, Enhanced CD107a expression frequency on CD19-drNK cells. drNK or CD19-NK cells were cocultured with medium alone or with the indicated cancer cells for 2 h at an E:T ratio of 1:1. Then, the percentage of $CD107a^+$ cells was measured by flow cytometry. The data represent means ± s.d. ($n = 3$). Statistical significance was determined by two-tailed Student's *t*-test. $^*P < 0.001$ (versus drNK cells).

Anticancer effects of drNK and CAR-drNK cells in vivo. The anticancer effects of drNK cells (Fig. 8a) and CAR-drNK cells (Fig. 8f) were further evaluated in BALB/c nude mouse xenograft models of human colon cancer lines (SW620 and COLO 205). To compare the anticancer effects of drNK cells with those of conventional NK cells, PBMC-NK and NK-92 cells and the anticancer agent doxorubicin, we injected mice subcutaneously with luciferase-expressing SW620 (SW620-Luc) cells (2×10^6), then injected them intravenously with PBS, low (5×10^6 cells; drNK cells-low) or high doses (1.5×10^7 cells; drNK cells) of drNK cells, high doses (1.5×10^7) of PBMC-NK cells or NK-92 cells, or doxorubicin (2 mg kg^{-1}) ($n=12$ per group), as indicated in Fig. 8a. The in vivo intensity of the bioluminescence imaging signals from the SW620 xenograft tumours receiving two infusions of drNK cells (days 1 and 4) (drNK cells-low and drNK cells) was significantly lower than that in tumours receiving the PBS control, in a dose- and time-dependent manner, without exogenous cytokine supply (Fig. 8b,c and Extended Data Fig. 4a). As expected, the tumour volume was significantly lower in mice that received the drNK cell infusion (182.09 ± 139.35 mm^3) than in PBS control mice ($1{,}369.97\pm440.16$ mm^3) (Extended Data Fig. 4b,c). Notably, administration of drNK cells, compared with conventional NK cells (PBMC-NK cells and NK-92 cells), more effectively decreased the tumour burden in SW620 xenograft mice (Fig. 8b,c and Extended Data Fig. 4a), thus indicating the superior anticancer activity of drNK cells in vivo.

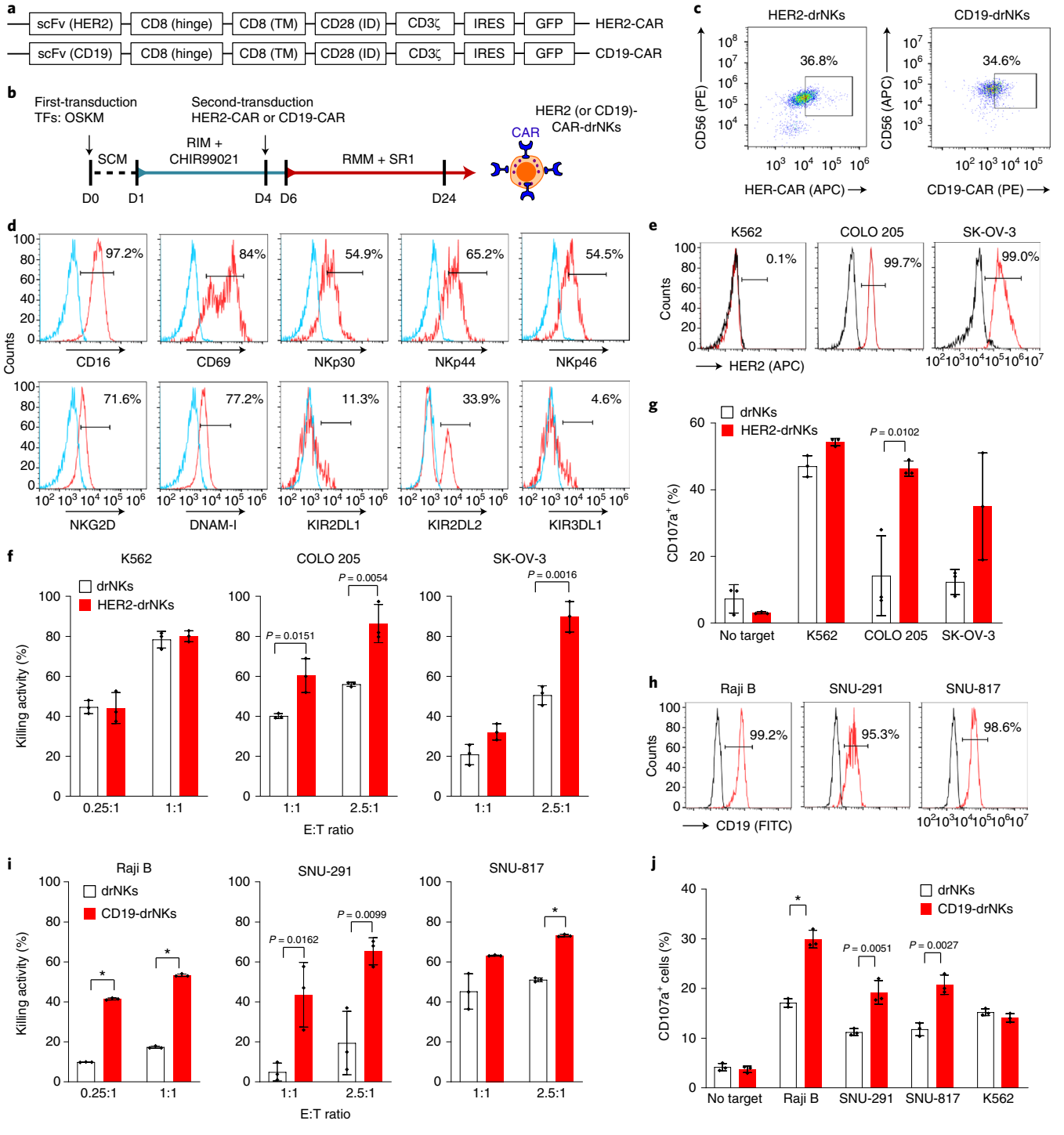

Because the in vivo efficacy of drNK cells in solid tumours relies on post-infusion persistence and infiltration levels, we next compared the in vivo persistence of the transferred drNK and PBMC-NK cells and examined the distribution of drNK cells in the SW620 xenograft tumours. To assess the persistence of drNK, we collected blood from the tail veins of mice injected with 1.0×10^7 drNK or PBMC-NK cells on days 7, 14 and 21. Higher numbers of hCD45$^+$hCD56$^+$ human NK cells were retrieved from the drNK-injected mice ($1.6\times10^5\pm2.3\times10^4$ cells per ml ($n=6$) on day 7) than from the PBMC-NK-injected mice ($1.3\times10^5\pm4.2\times10^4$ cells per ml ($n=6$) on day 7) (Fig. 8d), thus suggesting a better in vivo persistence of drNK cells than PBMC-NK cells. After injection of drNK cells labelled with DiR into SW620 xenograft mice, drNK homing and infiltration in tumours were additionally revealed by fluorescence imaging of the DiR$^+$ drNK cells (Extended Data Fig. 4d). Finally, we found that the drNK cell treatments, compared with other treatments (PBS control, PBMC-NK cells and NK-92 cells), significantly improved the survival rates of the SW620 tumour-bearing mice (Fig. 8e).

Given the promising in vitro results (Fig. 7), we next evaluated the in vivo anticancer effects of the HER2-CAR drNK cells in HER2-positive COLO 205 colon cancer xenograft mice (Fig. 8f and Extended Data Fig. 5c). The mice injected subcutaneously with luciferase-expressing COLO 205 (COLO 205-Luc) cells were injected intravenously with PBS or drNK cells, HER2-CAR drNK cells, NK-92 cells or HER2-CAR NK-92 cells ($n=12$ per group) (Fig. 8f and Extended Data Fig. 5c). As revealed by a lower bioluminescence imaging intensity than in mice treated with PBS control ($5.8\times10^{10}\pm2.2\times10^9$ radiance; day 35) and drNK cells ($6.1\times10^9\pm5.9\times10^8$ radiance; day 35), HER2-CAR drNK cells ($2.9\times10^9\pm4.1\times10^8$ radiance; day 35) exhibited a remarkably enhanced capability to suppress tumour burden in SW620 xenograft tumours (Fig. 8g,h and Extended Data Fig. 5a,b). In addition, the survival rate of COLO 205 colon cancer-bearing mice was significantly improved in HER2-CAR drNK cell-treated groups compared with non-CAR drNK cell-treated groups (Fig. 8i). Although both HER2-CAR drNK cells and HER2-CAR NK-92 cells inhibited tumour growth more effectively than their counterpart non-NK cells in COLO 205 xenograft mice, the HER2-CAR NK-92 cells showed greater efficacy (Extended Data Fig. 5c–f). Together, these in vivo data demonstrate the HER2-specific cancer-killing effects of HER2-CAR drNK cells on COLO 205-Luc tumours.

Discussion

Achieving therapeutically optimal levels of NK cells, in terms of functionality, accessibility, scalability and safety, is critical to meet the growing clinical demands for efficacious NK immunotherapy. Our data revealed that functionally competent drNK cells, as well as cancer antigen-specific CAR-redirected drNK cells, can be easily and efficiently produced using a core set of OSKM pluripotency transcription factors, which effectively trigger an initial wave of cell fate conversion to other specific lineages[40,41]. In particular, as key lineage-determining stimulators, Wnt agonist CHIR99021 and AhR antagonist SR1 are critically required for efficient drNK cell production. Our data suggest that CHIR99021 potently decreases the heterogeneity of OSKM-induced reprogramming intermediates by suppressing myeloid lineage commitment, and the suppression of AhR signalling driven by both OSKM transient expression[29,30] and AhR antagonism is critical in enhancing complete drNK cell reprogramming.

drNK cells can be produced from various starting cell types, including lineage-related peripheral blood-derived cells and lineage-unrelated fibroblasts (data not shown), but at different efficiency levels. Among the tested cells, PBMCs and PBMC T cells with relatively high proliferative potential were found to be favourable for efficient drNK cell production. PCR-based *TCRB* clonality assay revealed that T cell-derived drNK cells are heterogeneous and non-clonal. In addition, re-expression of TCR chains, related to the risk of graft-versus-host disease, was not detected in T cell-derived drNK cells. Without extra differentiation and feeder cell support, clinical-scale, highly pure CD56^{bright}CD16^{bright} drNK cells (~8,300-fold increase over starting cell numbers; purity > 97% CD56$^+$CD3$^-$) can be obtained with PBMCs or PBMC T cells within 24–28 reprogramming days and can be further expanded for approximately 30–40 d without loss of the original properties of the cells.

The iPSC-NK strategy provides important advantages, such as easy generation of genetically modified NK cells (for example, CAR-NK cells) and the ability to use a clonal master iPSC cell bank for off-the-shelf therapy. Multiple differentiation and expansion processes using genetically modified feeder cells are currently indispensable for the production of scalable NK cells[19,42,43]. In parallel with conventional NK sources, drNK cells may provide an important alternative for the production of a broad array of autologous and allogeneic CD56^{bright}CD16^{bright} NK products (both normal and patient derived), particularly for the development of ready-to-use NK cells.

Studies have demonstrated that OSKM transcription factor-mediated lineage conversion involves dedifferentiation towards progenitor-like intermediates by bypassing a pluripotent state[40,44,45]. Although flow cytometry analysis did not detect stem cell-like CD34$^+$ intermediates, RT-PCR analysis indicated considerable, transient upregulation of haematopoietic progenitor-related genes at an early stage of drNK cell reprogramming. As expected, compared with those in iPSC intermediates (at reprogramming day 6), the levels of pluripotency-related gene expression in drNK cell intermediates (also at reprogramming day 6) were much lower, whereas the levels of haematopoietic progenitor-related gene expression were higher. Transient overexpression of pluripotency transcription factors may allow the cells to effectively respond to NK lineage-specifying culture conditions, and also enable

Fig. 8 | Anticancer activity of drNK and HER2-drNK cells in the in vivo xenograft model. a, Experimental design of the in vivo anticancer activity assay of drNK cells. Mice bearing SW620-Luc xenografts were injected intravenously with PBS control, drNK cells (5.0×10^6 (drNK-low) or 1.5×10^7), PBMC-NK cells (1.5×10^7) or NK-92 cells (1.5×10^7) on days 1 and 4. As a control, doxorubicin (2 mg kg^{-1}) was injected intraperitoneally every other day for 2 weeks. **b**, Representative bioluminescence images of mice receiving the indicated treatments at the indicated days post SW620-Luc inoculation. **c**, Quantitative graph of the bioluminescence signals shown in **b** for day 21. The horizontal bars show mean values and the error bars represent s.d. Each symbol represents one mouse in each group ($n=10$–12 biological replicates per sample). Statistical significance was determined by two-tailed Student's *t*-test. **d**, Number of hCD45$^+$hCD56$^+$ cells in mice that received drNK or PBMC-NK cells, as analysed by flow cytometry. The data represent means ± s.d. ($n=3$ biological replicates for each sample). **e**, Kaplan–Meier analysis of survival. A log-rank (Mantel–Cox) test was used to determine the significance of the difference between the survival curves ($P=0.017$). **f**, Schematic of the in vivo anticancer activity assay of CAR-drNK cells. Mice bearing COLO 205-Luc xenografts were injected intravenously with PBS, drNK cells or HER2-drNK cells on days 1 and 4. **g**, Representative bioluminescence images of mice receiving the indicated treatments at the indicated days after COLO 205-Luc inoculation. **h**, Quantification of the bioluminescence signals shown in **g** at day 35. The horizontal bars show mean values and the error bars represent s.d. Each symbol represents one tumour xenograft in each group ($n=8$–9 biological replicates for each sample). Statistical significance was determined by two-tailed Student's *t*-test. *$P<0.001$ (versus control). **i**, Kaplan–Meier analysis of survival in the COLO 205 xenograft model. The statistical significance of the difference in survival rates was determined by a log-rank (Mantel–Cox) test ($P=0.040$).

reprogramming cells to proliferate and undergo lineage conversion into NK cells. In support of this possibility, PBMC-NK cells cultured with drNK cell reprogramming medium alone did not proliferate to the same extent as OSKM-transduced reprogrammed cells and did not acquire the same drNK cell CD56CD16 phenotype. Further detailed studies using cells originating from the same donor and sharing the same genetic background are required to: confirm the phenotypic and functional equivalence of drNK cells and conventional NK cells; fully elucidate the identity and state of reprogramming intermediates; and clarify whether drNK cells are a product

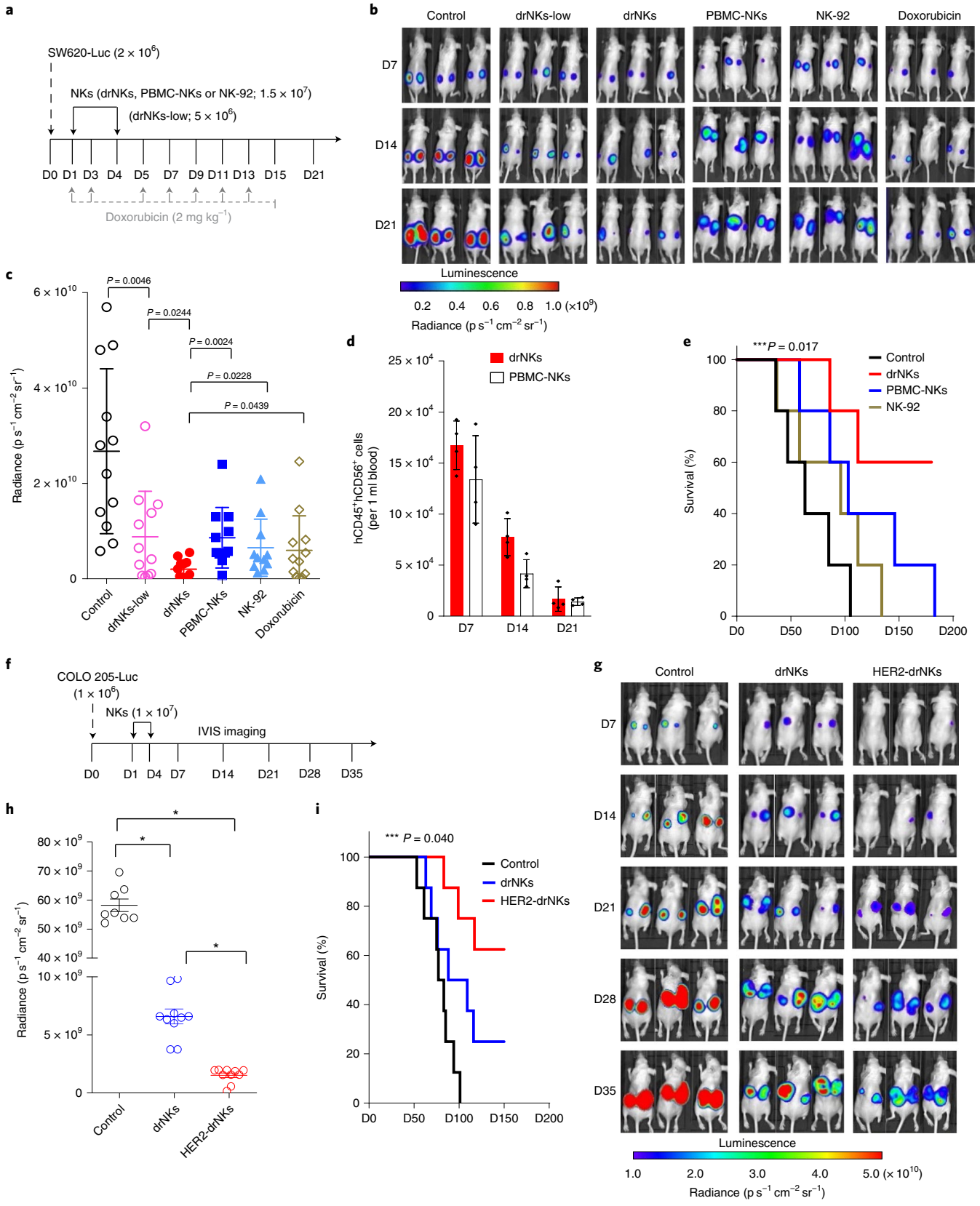

of directed differentiation from the transient progenitor-like state occurring during reprogramming process.

A hallmark of CD56^{bright}CD16^{bright} drNK cells is their function as strong anticancer effectors that exert a broad range of cytotoxic activities against various haematological and solid cancer cells, including blood, brain, breast, colon, liver, lung, ovarian, pancreatic and prostate cancer cells. Our in vitro and in vivo functional assays showed that drNK cells appear to be functionally more competent than freshly isolated CD56^{dim} NK cells (PBMC-NK and UCB-NK cells) in anticancer immune responses, including cytokine secretion (IFN-γ, granzyme B and TNF-α), lytic granule exocytosis (CD107a) and cancer-killing cytotoxicity. In a mouse colon cancer xenograft model, transplantation of drNK cells, compared with PBMC-NK and NK-92 cells, decreased the tumour burden and prolonged survival more effectively. Notably, drNK cells expressing high levels of NKG2D—a major recognition receptor for targeting and killing CSCs[46]—effectively eradicated CSCs in 3D in both in vitro and in vivo models, thus suggesting their potential in applications for CSC-directed cancer therapy[5,47].

Importantly, the anticancer efficacy of drNK cells was effectively enhanced by combining other anticancer modalities, including ADCC-mediating therapeutic antibodies and CAR introduction, which mediate the targeted killing of cancer-specific antigen-producing cancer cells. In the absence of target cells, an artificial in vitro ADCC assay using rituximab-mediated CD16 engagement and agonistic anti-KLC confirmed the superior ADCC activity of drNK cells over PBMC-NK cells—an effect that appears to correlate with their higher CD16 expression and activation of downstream PI3K/AKT signalling[48]. We also determined that an anti-EGFR ADCC antibody (cetuximab) potently triggered drNK cell-mediated ADCC activity against EGFR^{+} colon cancer cells in a selective manner. NK-92 (ref. [49]) and iPSC-NK cells[42] typically express no or low levels of ADCC-related CD16, thus indicating a lack of ADCC activity. Genetic modifications to improve CD16 expression have been used to complement their ADCC effector function[18,20,49].

We showed that CAR-CD19 or CAR-HER2 expression by reprogramming culture strongly improves the anticancer effects of drNK cells against CD19- or HER2-expressing cancer cells, respectively. Transplantation of CAR-HER2-drNK cells, compared with transplantation of drNK and HER2-NK-92 cells, considerably increased the anticancer responses in a mouse HER2-positive colon cancer xenograft model. Our findings also revealed important adaptive immune features of drNK cells, such as a memory-like function[50] and crosstalk with major antigen-presenting cells such as T cells[51,52]. We showed that memory-like drNK cells with enhanced effector functions and anticancer activity can be induced by short-term cytokine pre-stimulation, as previously described[38]. We also demonstrated that soluble factors secreted from resting and cancer cell-activated drNK cells potently activate T cells in vitro. In a mouse model in vivo, intraperitoneal delivery of drNK cells effectively recruited T cells into the peritoneal cavity, whereas T cells were depleted from peripheral blood, thus suggesting the ability of drNK cells to produce T cell-recruiting chemokines. In further support of these findings, we showed that drNK cells positively contribute to T cell infiltration into tumours, thereby enhancing anticancer activity in a colon cancer xenograft model (Extended Data Fig. 6).

In summary, our drNK cell strategy provides an easy and rapid route for the production of autologous and allogeneic NK/CAR-NK products with a CD56^{bright}CD16^{bright} phenotype and excellent anticancer functionality from a broad range of human somatic cells, including normal and patient-derived diseased cells. The use of drNK cells may help to reveal the lineage relationship and hierarchies among distinct NK subsets in conjunction with their functionality and therapeutic utility, particularly in cancers. Our study shows the therapeutic potential of drNK cells against a wide range of cancers, including solid cancers with poor therapeutic options, and provides strong rationale for the development of drNK cell combination therapy to overcome limitations of conventional cancer therapy.

Methods

Animals. All animal experiments were performed in accordance with the guidelines of the Korea Research Institute of Bioscience and Biotechnology (KRIBB) Institutional Animal Care and Use Committee (Animal Welfare Assurance Number: KRIBB-AEC-19260).

Human primary cells. For PBMC preparations, whole-blood samples from healthy donors were supplied by the blood centre of the Korean Red Cross, Republic of Korea in accordance with the guidelines established by the Institutional Review Board of KRIBB (number P01-201812-31-010). The PBMCs were isolated using Ficoll–Hypaque density gradient centrifugation with Ficoll–Hypaque lymphocyte isolation medium. PBMCs were cultured in StemPro-34 SFM medium containing 2.5% StemPro-34 nutrient supplement, 1% penicillin/streptomycin (Thermo Fisher Scientific), 2 mM GlutaMAX I (Thermo Fisher Scientific), 20 ng ml^{-1} human IL-3 (Peprotech), 20 ng ml^{-1} human IL-6 (Peprotech), 100 ng ml^{-1} human SCF (Peprotech) and 100 ng ml^{-1} human FLT3L (Peprotech).

The NK cells were purified from PBMCs or primary human UCB mononuclear cells (STEMCELL Technologies) by negative selection using a MACS NK Cell Isolation Kit (Miltenyi Biotec) according to the manufacturer's protocol. Briefly, 1×10^7 cells were suspended in 40 µl binding buffer containing 2% bovine serum albumin (BSA; Sigma–Aldrich) and 1 mM EDTA (Thermo Fisher Scientific) in PBS. Then, 10 µl biotinylation reagent was added and incubation was performed at 4 °C. After 5 min, 30 µl binding buffer and 20 µl microbeads were added and incubation was performed for an additional 10 min at 4 °C. The mixture was diluted with 500 µl binding buffer and poured into a mini magnetic column. The flow through was centrifuged for 5 min at 300*g*. The cell pellets were resuspended and cultured in RPMI 1640 (Thermo Fisher Scientific) containing 200 IU ml^{-1} IL-2, 1% penicillin/streptomycin and 10% foetal bovine serum (FBS; Thermo Fisher Scientific). For long-term culture, the purified NK cells were cultured in RPMI 1640 medium containing 200 IU ml^{-1} IL-2 and 10% FBS or 200 IU ml^{-1} IL-2, 10 ng ml^{-1} human IL-15 and 10% FBS. Fresh medium was replaced every 2–3 d. NK-92 cells were cultured in RPMI 1640 containing 10% FBS and 200 IU ml^{-1} IL-2, and fresh medium was replaced every 2–3 d.

CD3^{+} T cells, monocytes or B cells were isolated from PBMCs using the Pan T Cell Isolation Kit (Miltenyi Biotec), Pan Monocyte Isolation Kit (Miltenyi Biotec) or B Cell Isolation Kit (Miltenyi Biotec) according to the manufacturer's protocol. Briefly, similar to the NK cell isolation method, they were isolated from PBMCs using each biotinylating reagent. CD34^{+} cells were isolated from PBMCs using CD34^{+} microbeads, and the flow-through fraction comprised CD34^{-} cells. CD3^{-} cells were collected as the flow-through fraction using CD3 MicroBeads. CD3^{-}CD56^{-} cells were isolated from the CD3^{-} flow-through cell fraction using CD56^{+} microbeads. CD34^{-}CD56^{-} cells were obtained from CD34^{-} cells using CD56^{+} microbeads.

Direct reprogramming to drNK cells or CAR-drNK cells. As depicted in Fig. 1a, starting cells (PBMCs or PBMC subsets; $1–3 \times 10^5$ cells) were transduced in starting cell medium (StemPro-34 serum-free medium, 2.5% StemPro-34 nutrient supplement, 1% penicillin/streptomycin, 2 mM GlutaMAX I, 20 ng ml^{-1} human IL-3, 20 ng ml^{-1} human IL-6, 100 ng ml^{-1} human SCF and 100 ng ml^{-1} human FLT3L) with Sendai virus carrying human OCT4, SOX2, KLF4 and c-Myc (CytoTune 2.0 Reprogramming Kit) at various multiplicity of infection values (0–10 MOI) with same ratio (KOS:K:M = 5:3:5) according to the manufacturer's recommendations (day 0). The next day (day 1), the OSKM-transduced cells were cultured in RIM (10% FBS, 1% penicillin/streptomycin, 20 ng ml^{-1} human IL-3, 20 ng ml^{-1} human IL-6, 25 ng ml^{-1} human SCF, 25 ng ml^{-1} human FLT3L and 25 ng ml^{-1} human TPO (Peprotech) in StemSpan SFEM II) with or without 1–5 µM CHIR99021 (Tocris) and 2 µM SR1 (Cellagen Technology) for 1–10 d. Then, the cells were further incubated with RMM (10% FBS, 1% penicillin/streptomycin, 200 IU ml^{-1} IL-2, 20 ng ml^{-1} human IL-7 (Peprotech), 20 ng ml^{-1} human IL-15 (Peprotech), 25 ng ml^{-1} human SCF and 25 ng ml^{-1} human FLT3L in StemSpan SFEM II) with or without 2 µM SR1 and 300 nM FICZ (Tocris) for 15–24 d. The established drNK cells were cultured and expanded in NK medium (10% FBS, 200 IU ml^{-1} IL-2 and 10 ng ml^{-1} human IL-15 in RPMI 1640) with medium changes every 3–5 d. For the generation of CAR-drNK cells, starting cells were co-transduced with Sendai virus carrying human Oct4, Sox2, Klf4 and c-Myc and lentiviral vectors carrying CAR constructs (CD19-CAR or HER2-CAR) (Fig. 7a) and incubated with RIM containing 5 µM CHIR99021 and then with RMM containing 2 µM SR1 (Fig. 7b).

Human cancer cells. Human brain (SK-N-BE and U373MG), breast (MCF-7 and SK-BR-3), colon (HCT116, SW480 and SW620), liver (Hep3B and HepG2), lung (A549 and NCI-H460), ovarian (SK-OV-3), pancreatic (MIA PaCa-2) and prostate cancer cell lines (DU145, LNCap and PC-3) were obtained from the American Type Culture Collection and cultured in culture medium A (DMEM, 10% FBS and 1% penicillin/streptomycin). SNU-291 and SNU-817 cells were obtained from

the Korea Cell Line Bank, and human blood cancer cell lines (K562, SNU-291, Raji, SNU-817 and THP1) were cultured in culture medium B (RPMI 1640, 10% FBS and 1% penicillin/streptomycin). For the CSC spheroid preparation, SW620 cells were cultured in suspension with serum-free CSC medium (DMEM/F-12, 1% penicillin/streptomycin, 10 ng ml^{-1} basic fibroblast growth factor, 20 ng ml^{-1} epidermal growth factor and 2% B27) for 10 d with one-half of the medium changed every 3 d, as described previously[32]. For the functional assay, the CSC spheroids were dissociated into single cells with 0.25% trypsin/EDTA.

CAR constructs. The CD19-CAR construct was produced from the pHR CD19-empty CAR (Addgene; 113015), where the CD28 (NM_006139.3) intracellular domain, CD3ζ (NM_000734.3) domain and IRES were sequenced between the CD28 intermembrane domain and enhanced GFP sequence. The HER2-CAR construct was generated by replacing the CD19-scFv sequence of the CD19-CAR construct with the nucleotide sequence encoding the ErbB2-specific scFv (FRP5) antibody. Each domain was synthesized, and lentiviral CAR constructs were produced through overlap PCR (Gibson Assembly).

For lentiviral production, HEK293T cells seeded in 90-mm culture dishes (0.8×10^7 cells per dish) in 10 ml DMEM containing 10% FBS were transfected using 293Expresso Transfection Reagent (Excellgen) according to the manufacturer's instructions. Viruses were harvested after 72 h and clarified by filtration using a 0.45-μm filter and concentrated by centrifugation at 25,000 r.p.m. for 150 min. The viral pellets were resuspended in RPMI 1640 medium. The number of transducing units was evaluated in HEK293T cells using the limiting dilution method. Briefly, HEK293T cells were seeded in six-well plates at 5×10^5 cells per well. The next day, the concentrated viral particles were used to generate tenfold serial dilutions by adding 15 μl virus to 135 μl culture medium. Then, 100 μl diluted virus was transferred to each well, which was replaced with 1 ml culture medium containing 4 μg ml^{-1} Polybrene (Santa Cruz Biotechnology). The medium was replaced with fresh culture medium the next day. At 48 h after infection, fluorescence-activated cell sorting analysis was performed, and cells with 10–20% GFP positivity were selected for titre calculation. The titre was calculated as follows: transduction units per ml = (cell number in each well before infection × percentage of GFP-positive cells)/(0.1 × dilution fold).

RT-qPCR. Total RNA was extracted using an RNeasy Mini kit (Qiagen) and reverse transcribed using a SuperScript VILO cDNA Synthesis Kit (Thermo Fisher Scientific) according to the manufacturer's instructions. Quantitative PCR was performed with SYBR Green and analysed using a 7500 Fast Real-Time PCR system (Applied Biosystems). All primers were synthesized by Genotech (Republic of Korea). The primers are described in Supplementary Table 1.

Haematopoietic colony formation assay. The OSKM-transduced cells (1×10^5 cells) were cultured with RIM in the presence of 0.1% dimethyl sulfoxide (DMSO; Sigma–Aldrich) and 2 μM IWP2 (Sigma–Aldrich), 10 μM XAV939 (Sigma–Aldrich) or CHIR99021 (1, 3 or 5 μM) for 5 d. For the colony formation assays, equal numbers of cells per six-well plate were cultured in semi-solid MethoCult H4435 Enriched medium (STEMCELL Technologies) for 14 d according to the manufacturer's protocol, and the colony numbers were counted under an inverted microscope.

Flow cytometry. The cells were washed twice with PBS, fixed with 2% formaldehyde in PBS for 10 min and washed three times with PBS. For cell-surface marker staining, the fixed cells were blocked with 0.5% BSA and 1 mM EDTA in PBS for 20 min at room temperature. For intracellular staining, the fixed cells were permeabilized with 0.5% Tween 20, 0.5% BSA and 1 mM EDTA in PBS for 20 min at room temperature. The cells were then incubated with fluorophore-conjugated primary antibodies or isotype controls in 1% BSA and 1 mM EDTA in PBS for 20 min at room temperature, washed with PBS and analysed using a BD Accuri C6 flow cytometer (BD Biosciences). Flow cytometric data were analysed using FlowJo software version 10.4.2. (Tree Star) and Prism 6.0 (GraphPad Software). The antibodies are described in Supplementary Table 2.

Cytotoxicity assay. NK cell cytotoxicity was evaluated using a calcein-AM release assay. The target cancer cells were suspended in RPMI culture medium (10% FBS), labelled with calcein-AM (Thermo Fisher Scientific), plated in 96-well plates and incubated in a 37 °C incubator (5% CO_2) for 1 h. The effector NK cells were then added at various E:T ratios as indicated. The plates were centrifuged at 400*g* for 1 min and incubated for the indicated times. Equal volumes of supernatants were taken from each well and transferred to new plates. The samples were analysed using a fluorescence plate reader (485 nm/535 nm). NK cell cytotoxicity (%) was calculated as follows: NK cell cytotoxicity (%) = ((measured value − minimum value)/(maximum value − minimum value)) × 100. In this equation, the minimum value is the measurement of a well in which only calcein-labelled target cells are present, and the maximum value is the measurement value of a well in which the cells have been completely lysed by the addition of 2% Triton X-100 (Sigma–Aldrich) to the calcein-labelled target cells.

Antibody-dependent cell cytotoxicity. To evaluate drNK cells induced by CD16 participation in the presence of therapeutic antibodies in drNK and PBMC-NK cells, we used rituximab (Bio-Rad) and anti-human KLC (Sigma–Aldrich), as previously described[34]. Briefly, 1.0×10^6 NK cells per sample (100 μl RPMI 1640) were incubated with rituximab (100 μg ml^{-1} in RPMI 1640) on ice for 30 min, then the cells were washed with cold NK medium (NK medium = RPMI 1640 containing 200 IU ml^{-1} IL-2, 1% penicillin/streptomycin and 10% FBS). These cells were immediately incubated with 50 μl pre-warmed NK medium containing KLC (50 μg ml^{-1}) at 37 °C. After stimulation with or without KLC, the cells were analysed by immunoblotting, RT-qPCR and flow cytometry.

To measure ADCC in drNK cells, the target cells labelled with calcein-AM were incubated with serial dilutions of cetuximab (Bio-Rad)—a human EGFR monoclonal antibody—for 30 min at room temperature. The effector NK cells were added and incubated in a 37 °C incubator (5% CO_2) for 2 h. The ADCC was calculated as follows: ADCC (%) = ((measured value with antibody − measured value without antibody)/(maximum value − minimum value)) × 100. The antibodies are described in Supplementary Table 1. For analysis of IFN-γ secretion by cetuximab-activated drNK cells, 1×10^5 drNK cells were cultured with cetuximab-coated colon cancer cells (HCT116, SW480 and SW620) for 2 h at an E:T ratio of 1:1. The percentage of IFN-γ$^+$ cells was measured by flow cytometry.

Western blot analysis. The cells were lysated in RIPA buffer (150 mM sodium chloride, 1% Triton X-100, 0.5% deoxycholic acid, 0.1% sodium dodecyl sulfate and 50 mM Tris–HCl (pH 8.0)), and protein lysates (20 μg protein) were separated by sodium dodecyl sulfate polyacrylamide gel electrophoresis and transferred onto a polyvinylidene difluoride membrane. After blocking in 5% BSA in Tris-buffered saline containing 0.05% Tween 20 for 30 min, the membranes were incubated with the indicated primary antibodies pAKT (Ser473; Cell Signaling Technology), pERK (Cell Signaling Technology) and β-actin (Abcam) for 1 h or overnight, washed and incubated with horseradish peroxidase-conjugated secondary antibodies. The immunoreactive bands were visualized using enhanced chemiluminescence solution (Thermo Fisher Scientific).

Enzyme-linked immunosorbent assay (ELISA). For determination of the concentrations of secreted IFN-γ, TNF-α and granzyme B, commercial ELISA kits (Abcam) were used according to the manufacturer's protocol.

Cytokine-induced memory-like NK cells. Memory-like NK cells were induced by cytokine stimulation, as depicted in Fig. 4d. The NK cells cultured with RPMI 1640 containing 10% FBS and low IL-15 (1 ng ml^{-1}; basal cytokine medium) for 1 week were incubated with either the control cytokine medium or cytokine medium A (RPMI 1640, 10% FBS, 10 ng ml^{-1} IL-12, 50 ng ml^{-1} IL-15 and 100 ng ml^{-1} IL-18) for 16 h. After three washes with RPMI 1640 containing 10% FBS, the cells were further cultured in basal cytokine medium with one-half of the medium changed every other day. After 1 week, the NK cells were restimulated by culturing them with cytokine medium B (RPMI 1640, 10% FBS, 10 ng ml^{-1} IL-12 and 50 ng ml^{-1} IL-15) for 4 h or culturing them with K562 cells (1:1 ratio). Then, their memory-like ability was determined by the level of cytokine (IFN-γ) secretion.

T cell activation. The conditioned medium was prepared from supernatants derived from single cultures of either drNK (drNK-CM) or SW620 cells (SW620-CM) or cultures comprising both drNK cells and SW620 cells (at a 1:1 ratio; drNK–SW620-CM) seeded at 1×10^7 cells per 100-mm culture dish in 10 ml culture medium. After 24 h of incubation, the culture medium was collected, centrifuged at 300*g* for 5 min and filtered through a 0.22-μm filter. For T cell activation, 1 ml of each conditioned medium collected was added to the CD3$^+$ T cells (1×10^6 cells) and incubated for 16 h. The conditioned medium-mediated activation of T cells was analysed by observing the expression of the activation marker CD69 by flow cytometry.

T cell recruitment assay. BALB/c nude mice were injected intravenously with T cells (1.0×10^7 cells) preactivated with drNK–SW620-CM for 16 h and intraperitoneally with PBS or drNK cells (1.5×10^7 cells) on the same day. After 4 d, peripheral blood (200 μl) was collected from the retro-orbital vein and treated with heparin. The red blood cells were lysed with ACK lysing buffer (Thermo Fisher Scientific) for 10 min at room temperature. After three washes with PBS, the cells were suspended in 200 μl of PBS containing 0.5% BSA and 1 mM EDTA. After 4 d, the mice were sacrificed, and the cell populations of their peritoneal cavities were isolated with PBS injection (4 ml) as described previously [53]. The peritoneal cells were suspended in 1 ml of PBS containing 0.5% BSA and 1 mM EDTA. The numbers of CD3$^+$ T cells in the 50 μl samples from peripheral blood and peritoneal cavity were analysed by flow cytometry.

Time-lapse confocal imaging. GFP-expressing SW620 cells were cultured to form GFP-SW620 CSC spheroids (GFP-SW620 spheroids) as indicated above. Spheroids seeded and cultured on Matrigel-coated silicon culture inserts for 16 h were further cultured with or without drNK cells for 24 h. The number of cells in spheroids (mean values) was determined by trypsinizing 6–10 spheroids, staining with Trypan blue and counting the number of viable cells. Time-lapse images were captured using an IX83 microscope in a 37 °C incubator (5% CO_2) for 24 h. Time-lapse images were taken every 5 min with a 10x objective and analysed

using Cellsens software and ImageJ software. For confocal imaging, the cells were fixed with 4% formaldehyde (Sigma–Aldrich) for 10 min and then washed with PBS two times. The cells were blocked with 0.5% BSA in PBS for 20 min at room temperature and incubated in PBS containing 0.5% BSA with CD56-PE and CD107a-APC for 20 min at room temperature. Images were obtained using an LSM800 confocal microscope (Zeiss), and 3D reconstruction was performed using ZEN lite 2.1 software (Zeiss).

Anticancer effects in a colon cancer xenograft model in vivo. BALB/c nude mice were injected subcutaneously with SW620 cells (2.0×10^6 cells) and intravenously with PBS or drNK cells (1.5×10^7 cells). For determination of the CSC incidence in SW620 xenograft tumours, the xenograft tumours were harvested 4 d after PBS or drNK injection, dissociated by trypsin/EDTA for 30 min at 37 °C and analysed by flow cytometry. For the tumour cell colony formation assay of the SW620 cancer xenografts, single cells (1×10^4 cells) from the tumour tissues of the SW620 cancer xenografts injected with PBS or drNK cells were cultured on six-well plates in DMEM supplemented with 10% FBS for 10 d and stained with 0.5% crystal violet before the viable clonal colonies were counted.

NOD/SCID mice were used as the xenograft model. SW620-Luc cells were generated using a lentiviral vector encoding GFP and luciferase. GFP-positive SW620-Luc cells (2×10^6) were sorted and injected subcutaneously into the back skin of 6–12 mice per group (day 0). NK cells (drNK cells = 5×10^6 (drNK-low), drNK cells = 1.5×10^7 (drNK-high), PBMC-NK cells = 1.5×10^7 or NK-92 cells = 1.5×10^7 in 150 µl of PBS) or PBS (150 µl) were injected intravenously into the lateral tail vein twice: on day 1 and on day 4. As a control, doxorubicin (2 mg kg^{-1}) was injected intraperitoneally every other day for 2 weeks. Tumour growth was monitored by bioluminescence analysis in vivo after an intraperitoneal injection of 150 µl D-luciferin (Promega) dissolved in PBS (150 µg ml^{-1}; Promega) using an IVIS 100 imaging system. For monitoring of the distribution of drNK cells in vivo, 1.0×10^7 drNK cells stained with DiR were injected intravenously 1 d after injection of SW620-Luc cells (2×10^6 cells). The xenograft tumours were harvested at 5 d. The tumour volume was measured in a blinded manner on day 28. The mouse survival mortality progressed to 180 d, at which time all mice in the experimental and control groups died. The resulting data were analysed using the Kaplan–Meier method.

For confirmation of the persistence of drNK cells in models in vivo, approximately 300 µl blood was collected from the retro-orbital vein of four mice injected with 1.0×10^7 drNK cells or PBMC-NK cells and treated with 25 µl heparin. These blood cell samples were added to 2 ml red blood cell lysis buffer (ACK lysing buffer) and incubated for 10 min at room temperature. After three washes with PBS, the cells were suspended in 300 µl PBS containing 0.5% BSA and 1 mM EDTA, and the number of human CD45$^+$CD56$^+$ cells was counted by flow cytometry.

To demonstrate the antitumor activity of T cell recruitment in a xenograft model that recruited T cells and infiltrated solid tumours, the mice injected subcutaneously with SW620-Luc (2.0×10^6 cells) were injected intravenously with either PBS or 1×10^7 drNK cells, 5×10^6 activated T cells, 1×10^7 drNK cells plus 5×10^6 activated T cells ($n=6$ per group) on day. For monitoring of the infiltration of T cells in vivo, 5.0×10^6 activated T cells stained with DiR were injected intravenously 4 d after the injection of SW620-Luc cells. The xenograft tumours were harvested at 8 d to obtain IVIS images and for analysis by RT-qPCR.

Statistical analysis. The results are presented as means ± s.d. Student's unpaired *t*-tests were used for statistical evaluation and $P<0.05$ was considered significant. The Kaplan–Meier method was used to determine the survival curves. The log-rank (Mantel–Cox) test was used to compare the curves of the study groups with those of the controls. A probability value of $P<0.05$ was considered statistically significant.

Reporting Summary. Further information on research design is available in the Nature Research Reporting Summary linked to this article.

Data availability

The main data supporting the results in this study are available within the paper and its Supplementary Information. All data generated in this study, including source data and the data used to make the figures, are available from Figshare at https://figshare.com/s/93edb79d917acacdcd20. The microarray data are available from the Gene Expression Omnibus under accession number GSE132907. Source data are provided with this paper.

Received: 27 August 2020; Accepted: 22 June 2021;
Published online: 2 August 2021

References

1. Shimasaki, N., Jain, A. & Campana, D. NK cells for cancer immunotherapy. *Nat. Rev. Drug Discov.* **19**, 200–218 (2020).
2. Chiossone, L., Dumas, P. Y., Vienne, M. & Vivier, E. Natural killer cells and other innate lymphoid cells in cancer. *Nat. Rev. Immunol.* **18**, 671–688 (2018).
3. Guillerey, C., Huntington, N. D. & Smyth, M. J. Targeting natural killer cells in cancer immunotherapy. *Nat. Immunol.* **17**, 1025–1036 (2016).
4. Caligiuri, M. A. Human natural killer cells. *Blood* **112**, 461–469 (2008).
5. Tallerico, R. et al. Human NK cells selective targeting of colon cancer-initiating cells: a role for natural cytotoxicity receptors and MHC class I molecules. *J. Immunol.* **190**, 2381–2390 (2013).
6. Messaoudene, M. et al. Mature cytotoxic CD56^{bright}/CD16$^+$ natural killer cells can infiltrate lymph nodes adjacent to metastatic melanoma. *Cancer Res.* **74**, 81–92 (2014).
7. Cooper, M. A., Fehniger, T. A. & Caligiuri, M. A. The biology of human natural killer-cell subsets. *Trends Immunol.* **22**, 633–640 (2001).
8. Verneris, M. R. & Miller, J. S. The phenotypic and functional characteristics of umbilical cord blood and peripheral blood natural killer cells. *Br. J. Haematol.* **147**, 185–191 (2009).
9. Freud, A. G., Mundy-Bosse, B. L., Yu, J. & Caligiuri, M. A. The broad spectrum of human natural killer cell diversity. *Immunity* **47**, 820–833 (2017).
10. Shereck, E. et al. Immunophenotypic, cytotoxic, proteomic and genomic characterization of human cord blood vs. peripheral blood CD56^{Dim} NK cells. *Innate Immun.* **25**, 294–304 (2019).
11. Jacobs, R. et al. CD56^{bright} cells differ in their KIR repertoire and cytotoxic features from CD56^{dim} NK cells. *Eur. J. Immunol.* **31**, 3121–3127 (2001).
12. Jonges, L. E. et al. The phenotypic heterogeneity of human natural killer cells: presence of at least 48 different subsets in the peripheral blood. *Scand. J. Immunol.* **53**, 103–110 (2001).
13. Marcon, F. et al. NK cells in pancreatic cancer demonstrate impaired cytotoxicity and a regulatory IL-10 phenotype. *OncoImmunology* **9**, 1845424 (2020).
14. Alter, G. et al. Sequential deregulation of NK cell subset distribution and function starting in acute HIV-1 infection. *Blood* **106**, 3366–3369 (2005).
15. Silla, L. Double-bright (CD56^{bright}/CD16^{bright}) natural killer cell adoptive immunotherapy for SARS-CoV-2. *Br. J. Haematol.* **190**, e322–e323 (2020).
16. Liu, E. et al. Use of CAR-transduced natural killer cells in CD19-positive lymphoid tumors. *N. Engl. J. Med.* **382**, 545–553 (2020).
17. Tang, X. et al. First-in-man clinical trial of CAR NK-92 cells: safety test of CD33-CAR NK-92 cells in patients with relapsed and refractory acute myeloid leukemia. *Am. J. Cancer Res.* **8**, 1083–1089 (2018).
18. Li, Y., Hermanson, D. L., Moriarity, B. S. & Kaufman, D. S. Human iPSC-derived natural killer cells engineered with chimeric antigen receptors enhance anti-tumor activity. *Cell Stem Cell* **23**, 181–192.e5 (2018).
19. Zhu, H., Lai, Y. S., Li, Y., Blum, R. H. & Kaufman, D. S. Concise review: human pluripotent stem cells to produce cell-based cancer immunotherapy. *Stem Cells* **36**, 134–145 (2018).
20. Zhu, H. et al. Pluripotent stem cell-derived NK cells with high-affinity noncleavable CD16a mediate improved antitumor activity. *Blood* **135**, 399–410 (2020).
21. Rosa, F. F. et al. Direct reprogramming of fibroblasts into antigen-presenting dendritic cells. *Sci. Immunol.* **3**, eaau4292 (2018).
22. Xie, H., Ye, M., Feng, R. & Graf, T. Stepwise reprogramming of B cells into macrophages. *Cell* **117**, 663–676 (2004).
23. Szabo, E. et al. Direct conversion of human fibroblasts to multilineage blood progenitors. *Nature* **468**, 521–526 (2010).
24. Galat, Y. et al. Application of small molecule CHIR99021 leads to the loss of hemangioblast progenitor and increased hematopoiesis of human pluripotent stem cells. *Exp. Hematol.* **65**, 38–48.e1 (2018).
25. Cao, N. et al. Conversion of human fibroblasts into functional cardiomyocytes by small molecules. *Science* **352**, 1216–1220 (2016).
26. Roeven, M. W. et al. The aryl hydrocarbon receptor antagonist StemRegenin1 improves in vitro generation of highly functional natural killer cells from CD34$^+$ hematopoietic stem and progenitor cells. *Stem Cells Dev.* **24**, 2886–2898 (2015).
27. Angelos, M. G. et al. Aryl hydrocarbon receptor inhibition promotes hematolymphoid development from human pluripotent stem cells. *Blood* **129**, 3428–3439 (2017).
28. Hughes, T. et al. The transcription factor AHR prevents the differentiation of a stage 3 innate lymphoid cell subset to natural killer cells. *Cell Rep.* **8**, 150–162 (2014).
29. Ko, C. I. et al. Repression of the aryl hydrocarbon receptor is required to maintain mitotic progression and prevent loss of pluripotency of embryonic stem cells. *Stem Cells* **34**, 2825–2839 (2016).
30. Ko, C. I., Wang, Q., Fan, Y., Xia, Y. & Puga, A. Pluripotency factors and Polycomb group proteins repress aryl hydrocarbon receptor expression in murine embryonic stem cells. *Stem Cell Res.* **12**, 296–308 (2014).
31. Pegram, H. J., Andrews, D. M., Smyth, M. J., Darcy, P. K. & Kershaw, M. H. Activating and inhibitory receptors of natural killer cells. *Immunol. Cell Biol.* **89**, 216–224 (2011).
32. Chen, X. et al. High levels of SIRT1 expression enhance tumorigenesis and associate with a poor prognosis of colorectal carcinoma patients. *Sci. Rep.* **4**, 7481 (2014).
33. Ohtani, H. Focus on TILs: prognostic significance of tumor infiltrating lymphocytes in human colorectal cancer. *Cancer Immun.* **7**, 4 (2007).

34. Petriello, A. et al. Assessment of human natural killer cell events driven by FcγRIIIa engagement in the presence of therapeutic antibodies. *J. Vis. Exp.* https://doi.org/10.3791/61144 (2020).
35. Liu, S. D. et al. Afucosylated antibodies increase activation of FcγRIIIa-dependent signaling components to intensify processes promoting ADCC. *Cancer Immunol. Res.* **3**, 173–183 (2015).
36. Jonker, D. J. et al. Cetuximab for the treatment of colorectal cancer. *N. Engl. J. Med.* **357**, 2040–2048 (2007).
37. Ishikawa, T. et al. Phase I clinical trial of adoptive transfer of expanded natural killer cells in combination with IgG1 antibody in patients with gastric or colorectal cancer. *Int. J. Cancer* **142**, 2599–2609 (2018).
38. Romee, R. et al. Cytokine activation induces human memory-like NK cells. *Blood* **120**, 4751–4760 (2012).
39. Cerwenka, A. & Lanier, L. L. Natural killer cell memory in infection, inflammation and cancer. *Nat. Rev. Immunol.* **16**, 112–123 (2016).
40. Bar-Nur, O. et al. Lineage conversion induced by pluripotency factors involves transient passage through an iPSC stage. *Nat. Biotechnol.* **33**, 761–768 (2015).
41. Zhu, S., Wang, H. & Ding, S. Reprogramming fibroblasts toward cardiomyocytes, neural stem cells and hepatocytes by cell activation and signaling-directed lineage conversion. *Nat. Protoc.* **10**, 959–973 (2015).
42. Hermanson, D. L. et al. Induced pluripotent stem cell-derived natural killer cells for treatment of ovarian cancer. *Stem Cells* **34**, 93–101 (2016).
43. Zhu, H. & Kaufman, D. S. An improved method to produce clinical-scale natural killer cells from human pluripotent stem cells. *Methods Mol. Biol.* **2048**, 107–119 (2019).
44. Kim, J. et al. Direct reprogramming of mouse fibroblasts to neural progenitors. *Proc. Natl Acad. Sci. USA* **108**, 7838–7843 (2011).
45. Maza, I. et al. Transient acquisition of pluripotency during somatic cell transdifferentiation with iPSC reprogramming factors. *Nat. Biotechnol.* **33**, 769–774 (2015).
46. Grossenbacher, S. K., Canter, R. J. & Murphy, W. J. Natural killer cell immunotherapy to target stem-like tumor cells. *J. Immunother. Cancer* **4**, 19 (2016).
47. Sandel, M. H. et al. Natural killer cells infiltrating colorectal cancer and MHC class I expression. *Mol. Immunol.* **42**, 541–546 (2005).
48. Mace, E. M. Phosphoinositide-3-kinase signaling in human natural killer cells: new insights from primary immunodeficiency. *Front. Immunol.* **9**, 445 (2018).
49. Klingemann, H., Boissel, L. & Toneguzzo, F. Natural killer cells for immunotherapy—advantages of the NK-92 cell line over blood NK cells. *Front. Immunol.* **7**, 91 (2016).
50. Uppendahl, L. D. et al. Cytokine-induced memory-like natural killer cells have enhanced function, proliferation, and in vivo expansion against ovarian cancer cells. *Gynecol. Oncol.* **153**, 149–157 (2019).
51. Vivier, E. et al. Innate or adaptive immunity? The example of natural killer cells. *Science* **331**, 44–49 (2011).
52. Ray, A. & Dittel, B. N. et al.Isolation of mouse peritoneal cavity cells. *J. Vis. Exp.* **2010**, 1488 (2010).

Acknowledgements

We are grateful to I. Choi for insightful advice during the course of this investigation. This work was supported by the National Research Foundation of Korea (2020R1A2B5B02002252 and 2019M3A9H1103797), the National Research Council of Science and Technology (CRC-15-02-KRIBB) and the KRIBB Research Initiative Program (1711134084/KGM5502113).

Author contributions

H.-S.K. and Y.S.C. conceived of the study idea. H.-S.K., B.S. and J.Y.K. developed the methodology. H.-S.K., B.S., J.Y.K., C.L.S., J.E.J. and Y.S.C. performed the investigation. H.-S.K., B.S. and J.Y.K. performed the statistical analyses. Y.S.C. provided resources. H.-S.K. and Y.S.C. wrote the original draft of the manuscript. H.-S.K. and Y.S.C. reviewed and edited the manuscript. Y.S.C. acquired funding.

Competing interests

The authors declare no competing interests.

Additional information

Extended data is available for this paper at https://doi.org/10.1038/s41551-021-00768-z.

Supplementary information The online version contains supplementary material available at https://doi.org/10.1038/s41551-021-00768-z.

Correspondence and requests for materials should be addressed to Y.S.C.

Peer review information *Nature Biomedical Engineering* thanks Pin Wang and the other, anonymous, reviewer(s) for their contribution to the peer review of this work.

Reprints and permissions information is available at www.nature.com/reprints.

Publisher's note Springer Nature remains neutral with regard to jurisdictional claims in published maps and institutional affiliations.